https://doi.org/10.5194/egusphere-2026-4643
Preprint. Discussion started: 6 August 2026

Ocean Heat Transport Convergence Drives Regional Energy Imbalance in the Sunlit Ocean Layer

Gael Forget[1]

[1]Earth, Atmospheric and Planetary Sciences, Massachusetts Institute of Technology, 77 Massachusetts Avenue, Cambridge, 02139, MA, USA

Correspondence: Gael Forget (gforget@mit.edu)

Abstract. The sunlit ocean layer (SOL, 0-200m) is where ocean heat transport (OHT) interacts directly with radiative forcing, where temperature changes feed back on the atmosphere, and where impacts of global warming on marine life are concentrated. Below 200m, except for geothermal heating in the abyss, energy imbalance is entirely governed by OHT processes. For the SOL, we introduce the concept of SOL energy imbalance (SOL-EI), defined as a closed heat budget that separates air-sea heat uptake from OHT convergence on a 10-year timescale. SOL-EI is estimated globally and regionally over 1980-2022 with observational uncertainty quantification. Results reveal that recent changes in SOL warming patterns are generally controlled by OHT convergence rather than local air-sea heat flux, which instead tends to act as a regional feedback mechanism. Global SOL-EI accumulation is estimated as the convergence between global air-sea heat uptake and heat export through 200m depth. This global index reveals interdecadal variability, with near-zero values linked to volcanic and internal climate forcing, and unabated accumulation of 30-60 ZJ/decade over the past decade. A leading interdecadal oscillation pattern (IOP) is furthermore identified directly from SOL-EI maps, and then decomposed into regional OHT convergence and air-sea flux terms. Here again results show that OHT convergence acts mainly as the driving process, and air-sea flux as a regional feedback. Because our framework defines SOL-EI as a time-evolving equation for 10-year trends, it provides a unified lens for interpreting global change, interdecadal variability, and regional patterns in terms of known processes. In addition, the mapping of Argo data within OCCA2 operates on residuals computed relative to a time-evolving state estimate that provides closed heat budgets. This methodological innovation enhances interpretability as compared to other gridded Argo datasets. Uncertainty quantification within the OCCA2 family of estimates is readily extensible to other Argo mapping methods and to the pre-Argo period, via alternative computations of the residual term, as demonstrated here using the IAPv4 gridded data product.

1 Introduction

Global warming is primarily manifested as ocean warming, with over 90% of the heat added by human activities now stored in the ocean's depths (Levitus et al., 2012; Roemmich et al., 2015; von Schuckmann et al., 2023; Minière et al., 2023; Li

https://doi.org/10.5194/egusphere-2026-4643
Preprint. Discussion started: 6 August 2026

et al., 2023a; Cheng et al., 2024a, and references therein). The rate of global warming is often characterized as Earth Energy Imbalance (EEI , or Earth EI), viewed from the perspective of a global budget of energy or heat, which has been increasing over the past few decades (Bagnell and DeVries, 2021; Minière et al., 2023; Hakuba et al., 2024; Wu et al., 2025). EEI estimates are typically derived starting from either the top of the atmosphere or the sea surface (Trenberth et al., 2009; Meyssignac et al., 2019; Loeb et al., 2021; Hakuba et al., 2024).

In this paper we consider EEI from the perspective of the sunlit ocean layer (SOL), as delimited by the sea surface and 200m depth. The SOL has an outsized influence on (1) climate feedbacks involving air-sea interaction and the cryosphere, and (2) marine life which is most abundant in the SOL, acclimated to specific temperature ranges, and feeds back onto the global carbon cycle directly (Asch et al., 2019; Feng et al., 2021; Anderson et al., 2021; Sallée et al., 2021). The SOL's direct exposure to radiative forcing via the sea surface is its defining feature. Since radiative forcing does not reach depths below 200m (Fig. A11), the fate of EEI at greater depths is in contrast entirely determined by the interplay of ocean transport processes, aside from minor effects geothermal heating in the abyss (Piecuch et al., 2015).

The observed shift in near surface ocean temperature climatology since 1980 induces marine heatwaves at unprecedented levels, with potentially dire consequences on marine ecosystems that are raising great concern (Hansen et al., 2010; Sen Gupta et al., 2020; Scannell et al., 2020; Li et al., 2020). Warming in the tropical SOL is another example of already heightened risk, as it can boost tropical storms and atmospheric rivers (Knutson et al., 2021; Gonzales et al., 2019). Given such impacts, we see an urgent need to accurately estimate and precisely understand the fate of EEI within the SOL – the layer where it meets key ocean transports and pathways (Hersh et al., 2025; Song and Forget, under review, i; Jiang et al., in press).

The recent history and geography of SOL warming rates are the main target for detailed analysis in this paper. Additional emphasis is placed on the past decade that shows increased SOL warming while the underneath layer continues to warm rather steadily (Fig. 1). Gridded estimates naturally tend to converge across mapping methods during this period thanks to the quasi-global data constraint that Argo provides over the Ocean's upper 2000m since 2004 (red curves), as highlighted in Hakuba et al. (2024). A major advance in this paper, however, is that we attribute observed trends and climate variability to a combination of surface forcing and OHT as part of a closed heat budget estimated globally (blue curves in Fig. 1) and regionally (see below).

Our theoretical framework defines SOL-EI as an equation, the 10-year mean SOL-HB , which we then estimate over the Global Ocean and the 1980-2022 period (Figs. 2 to 6). By integrating the left-hand-side of the SOL-EI equation over time, one recovers the observed multi-decadal rise in SOL heat content, while filtering out year to year fluctuations via the 10-year running average applied to SOL-HB (Fig. 2, top panel, and Fig. 3 compared with Fig. A1). The right-hand-side of the $\int$ SOL-EI dt equation is the sum over time of air-sea heat flux (Q) minus OHT divergence. In the global integral, the latter corresponds to a flux across 200m depth and into the dark ocean layer underneath (Fig. 2, middle panel, blue curve). The underlying SOL-EI equation, without time integration, is shown in the bottom panel of Fig. 2 (thick curves).

To estimate and analyze SOL-EI , the paper introduces an innovative estimation method. It combines a closed heat budget estimate with a non-conservative term derived from residual differences to Argo profiles (2004-2022, see appendix A). Furthermore, beyond the Argo period and to further assess uncertainties, the non-conservative term is alternatively derived using the IAPv4 gridded data product over 1980-2022 (Cheng et al., 2024b). This is helpful to put recent decadal trends into

https://doi.org/10.5194/egusphere-2026-4643
Preprint. Discussion started: 6 August 2026

climatological context and because detailed error calculation using profile data before Argo is complicated by the paucity of ocean observations. Based on IAPv4's good agreement with other such estimates (Minière et al., 2023; Hakuba et al., 2024), it provides an adequate representative for gridded observational ocean climatologies. In both cases, whether using Argo profiles directly or the gridded IAPv4 climatology as an alternative over 1980-2022, the residual term is relatively small (Figs. 1,2 ,A6,A9,A10), which demonstrates the skill of OCCA2 closed heat budget estimates.

2 Results

Global SOL-EI

The globally integrated SOL-EI accumulation serves as an index for the global rate of EEI accumulation in the SOL (Fig. 2, bottom panel, red curves). Over the past decades, it has oscillated between near zero (periods centered around 1993 and 2008) and periods when it reached 30-60 ZJOULE/DECADE (around 1987, 2001, and 2015). Reduced global SOL-EI coincides with periods of significant climate variability and volcanic activity Kosaka and Xie (2013); England et al. (2014); Medhaug et al. (2017), including the 1991 major eruption of Mount Pinatubo, which has the effect of reducing EEI as a whole (Church et al., 2005; Vernier et al., 2011; Fyfe et al., 2013; Dogar et al., 2020; Minière et al., 2023). The high SOL-EI periods, in turn, are hypothesized to reflect unabated SOL-EI . They show enhanced rates of EEI uptake, as one would expect, but also enhanced EEI export through 200m depth (Fig. 2, blue curves). Hence, we immediately realize that it is essential to accurately account for both terms on the right hand side in order to properly attribute SOL-EI accumulation (on the left hand side).

The difference between OCCA2.2d (dashed) and OCCA2.2a (solid) in the bottom panel of Fig. 2 is the non-conservative term diagnosed from Argo over 2004-2022 (black curves in Fig. 1). The difference between IAPv4 and OCCA2.2a provides an alternative estimate for this non-conservative term over 1980-2022 (Figs. 1,2). These differences are generally relatively small, which means that overall errors in the closed heat budget are relatively small.

The SOL-EI maximum around 2015 (Fig. 2, bottom) provides a unique window into unabated SOL-EI near present time, with dense Argo data coverage that we shall exploit. On average over 2013:17, SOL-EI accumulation is 49.6 ZJoule/ decade in OCCA2.2D (Argo-adjusted), 55.4 in OCCA2.2A (closed heat budget), and 44.1 in IAPv4 (gridded data product). Over 85:09, it is 15.1 ZJoule/ decade in OCCA2.2A, and 24.0 in IAPv4. While observational uncertainties must increase before the Argo era, these results suggest that global mean SOL-EI accumulation during 2013:2017 is likely twice to four-times as large as the 1985:2009 long term average.

Total EEI accumulation computed from the sea floor to the sea surface, for comparison, is 60% larger during 2013:2017 than 1985-2009 (in both OCCA2.2A and IAPv4). Absolute values are slightly larger for IAPv4 than OCCA2.2A in both periods (86.9 vs 71.2 over 1985-2009, and 142.5 vs 113.9 over 2013:2017), due additional warming below 2000m (not shown). Presumably, this heat would have entered the Ocean before the period that OCCA2.2A simulates.

For the recent period, OCCA2's final estimate obtained by adjusting OCCA2.2A based on Argo is 124.7 over the whole ocean, with a split of 49.6 for the SOL and 69.6 for layers below 200m depth. This gives a ratio of SOL-EI accumulation to total ocean EEI accumulation of 39.8% in OCCA2.2D over 2013:2017. This ratio furthermore seems to have increased compared with the

https://doi.org/10.5194/egusphere-2026-4643
Preprint. Discussion started: 6 August 2026

1985:2009 average – going from 21.3% to 48.6% in OCCA2.2A, and from 27.1% to 30.9% in IAPV4. Firming up estimates of this ratio and its tendency is viewed as an important goal for climate research owing to the potential impacts of increasing SOL-EI on marine ecosystems and climate feedbacks.

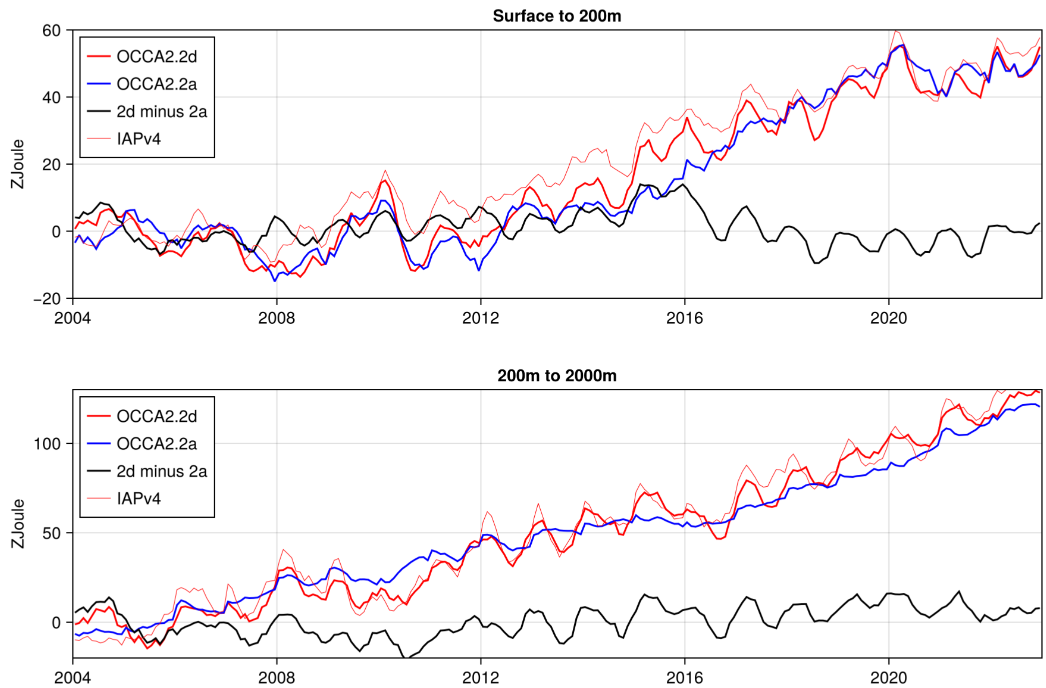

Figure 1. Top : heat content anomaly for 0-200m layer (SOL) as estimated in OCCA2.2 (red), by combining OCCA2.2A (blue) and the gridded difference between ARGO and OCCA2.2A (thin blue). Anomalies are computed with respect to the monthly 2004-2006 climatology, which filters out the seasonal cycle. Bottom : same but for the 200-2000m layer.

https://doi.org/10.5194/egusphere-2026-4643
Preprint. Discussion started: 6 August 2026

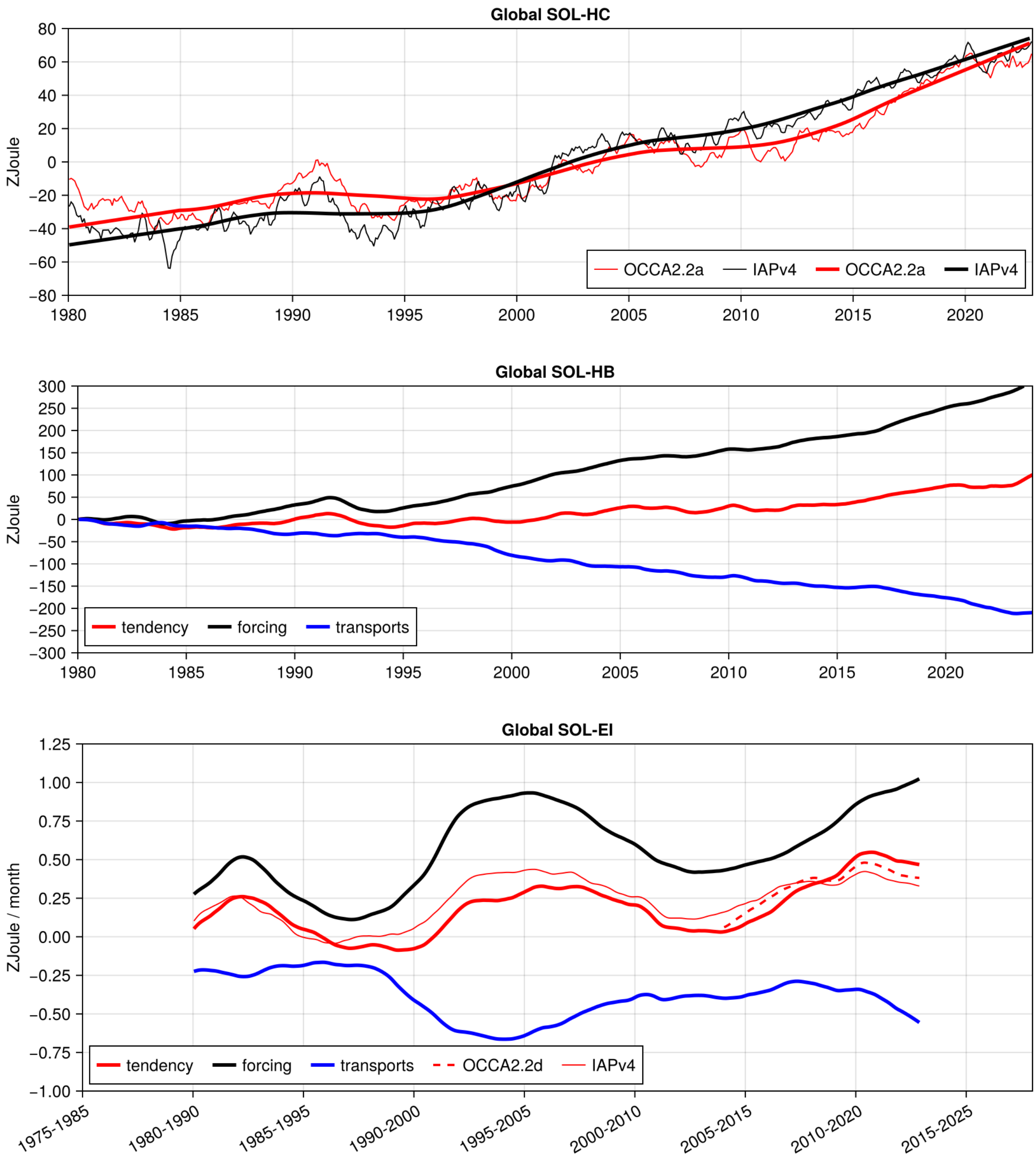

Figure 2. Top panel, thin curve : monthly heat content anomaly in the SOL estimated over 1980 to 2022. To filter out the mean seasonal cycle, a twelve-month smoother is applied before integrating temperature tendencies over time (Eq.A2). Top panel, thick curves : same calculation but using 10-year trends instead of monthly tendencies (Eq. A7). Middle panel : time integrated heat budget for the SOL in OCCA2.2A (Eq. A3). Bottom panel, thick curves : SOL energy imbalance (SOL-EI) defined as the ten-year mean SOL-HB in OCCA2.2A (Eqs. A5-A7). Thin curves : SOL-EI tendency term estimated from OCCA2.2 and IAPv4.

https://doi.org/10.5194/egusphere-2026-4643
Preprint. Discussion started: 6 August 2026

EEI below the SOL

The SOL is not only a site of EEI accumulation but also the conduit for EEI to reach deeper ocean layers via OHT as already noted (Fig. 2). Once EEI reaches below the SOL, its advent is almost entirely determined by OHT — solar radiation does not penetrate beyond 200m depth, and geothermal heating in the abyss remains a minor exception. At intermediate depths, EEI is found to accumulate the fastest at mid-latitudes, with maximum warming rates reaching 1000m depth near 40°S and 40°N (Fig. 3). While this general behavior was already known (Levitus et al., 2012; Li et al., 2023b), an interesting asymmetry emerges in Fig. 3. Over 1980-2007, southern warming outpaces northern warming at those depths (middle column, center and bottom rows), but the situation reverses in the recent period from 2007 to 2022, when northern mid-latitudes start to warm faster than southern mid-latitudes. There are multiple reasons why this could be the case, suggesting further research is needed beyond the scope of our study.

In the Northern Hemisphere, EEI accumulation is clearly surface intensified from 20°N to 80°N during the whole period – more so than in the Southern Hemisphere at the same latitudes based on Fig. 3. Poleward of 50°S , where Ekman transport drives a circumpolar OHT divergence, there is very little EEI accumulation at any depth (bottom right panels), which was already known (Frölicher et al., 2015; Armour et al., 2016; Song et al., 2025).

At lower latitudes, warming signals are propagating via known ocean transport pathways that tend to follow iso-density surfaces (Fig. 3, top panels). One such pathway follows a equatorward and westward route from the eastern side of ocean basins to the tropical flank of ocean gyres (Gu and Philander, 1997; Hersh et al., 2025). This route notably contributes to the global meridional overturning circulation and ocean heat transport (Forget and Ferreira, 2019; Rousselet et al., 2021; Wu and Gregory, 2022; Hersh et al., 2025; Li et al., 2023b). In the tropics, the progressive arrival of EEI via subsurface pathways is most evident in 2022 (top right panel), but the patterns of EEI accumulation are already present by 2007 based on our estimation (top middle panel; see also Levitus et al., 2012; Li et al., 2023b).

Finally, our analysis reveals that warming levels seen at mid-latitudes in 2007 (> 0.5 K) are found near the equator below the surface by 2022 (bottom left panels). This finding implies that 15 years is enough for EEI to transit from the subtropics ($\approx 35°$ latitude) to the equatorial band ($< 5°$ latitude) via the subsurface, consistent with well established transit mechanisms Gu and Philander (1997). Based on subtropical warming between 2007 and 2022 (bottom middle panels), we can thus project that subsurface temperature will rise by another 0.5 K or more in the tropics within the next 15 years.

https://doi.org/10.5194/egusphere-2026-4643
Preprint. Discussion started: 6 August 2026

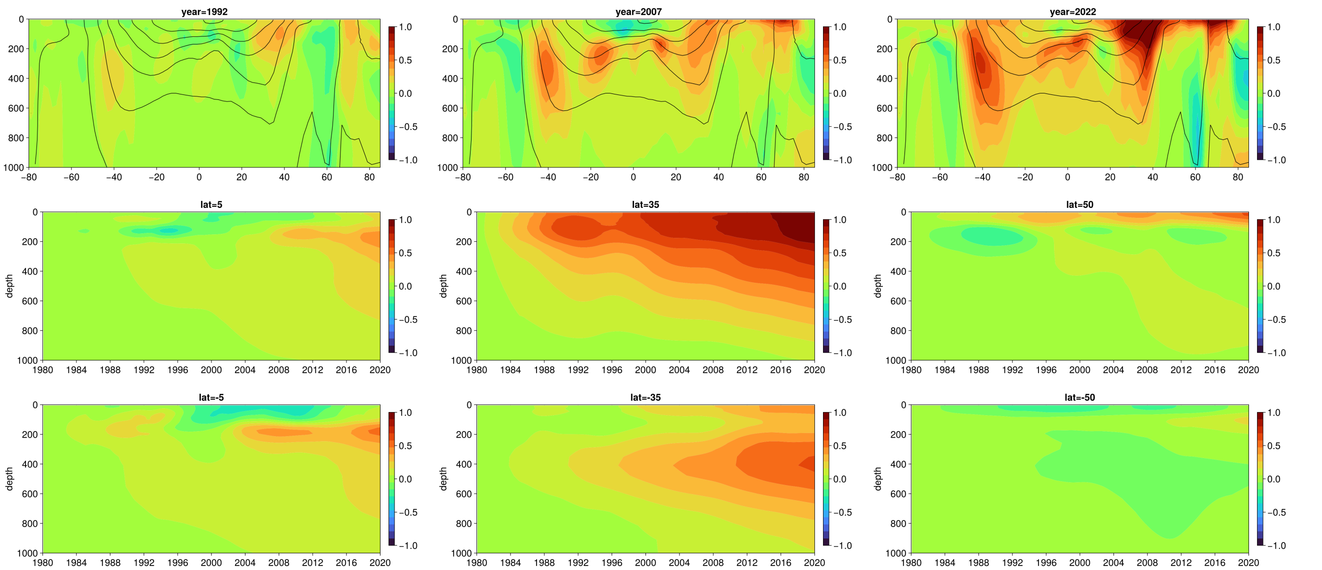

Figure 3. Cumulated Ocean EI in zonal mean view (Eq. A5) relative to the 1980-1982 climatology. Top : 1992 (left), 2005 (middle), and 2022 (right), with climatological iso-density contours shown in black. Middle panels : 5°N , 35°N , and 50°N . Bottom panels : 5°S , 35°S , and 50°S . Units: degree Celsius.

https://doi.org/10.5194/egusphere-2026-4643
Preprint. Discussion started: 6 August 2026

Relative SOL-EI

Within the SOL, surface intensified EEI accumulation is clear between 20°N to 80°N (Fig. 3, top right). This fact implies an increase in thermal stratification, which tends to inhibit convective mixing, and this positive feedback can lead to further increase in thermal stratification. In the Southern Hemisphere subtropics, surface intensified EEI accumulation is also identified between 20°S to 50°S more recently (bottom middle and top right panels). South of 50°S though, this phenomenon is not yet visible (bottom right panel), presubmably due to the prevalence of circumpolar OHT divergence and northward Ekman transport (Armour et al., 2016). A key question that remains to be addressed is whether this situation – the lack of surface intensified warming south of 50°S – will continue indefinitely.

Equally important is the lack of surface intensified EEI accumulation equatorward of 20 degree latitude between 1980 and 2022 (Fig. 3). We hypothesize that this is linked to the strongly divergent heat transport imparted by the winds near the equator (Forget and Ferreira, 2019). Divergent Ekman transport, linked to equatorial upwelling, would indeed inhibit local accumulation of tropical ocean heat uptake near the surface. But this damping mechanism ought to become less efficient moving forward as subsurface waters start to warm up near the equator as seen between 2007 and 2022 (Fig. 3). Such a scenario, if confirmed by future observations, is very alarming given the outstanding influence that tropical sea surface temperatures have on the climate system.

To further elucidate the geography of SOL-EI and its evolution in the recent period, it is useful to focus on anomalies computed relative to a mean reference state (Fig. 4). This CLIMATE NORMAL STATE (OR CNS) is estimated over the 1985-2009 period before the recent SOL warming maximum (Fig. 2). Specifically, CNS is estimated from the multidecadal OCCA2.2A solution (Fig. 2) via a weighted average of SOL-EI over 1985-2009 (section A5). Our estimation method jointly identifies a leading INTERDECADAL OSCILLATION PATTERN (OR IOP) , which is depicted along with the CNS warming pattern in Fig. 5.

To represent the recent period of unabated SOL warming, we select the average of SOL-EI over 2013:2017 based on Fig. 2. During this period, SOL-EI accumulation exceeds $1W/m^2$ over vast regions of the Ocean (Fig. 4, top panel). In contrast, CNS is characterized by regional warming rates generally below $0.5W/m^2$ (Fig. 5, top left). Hence, subtracting CNS from absolute SOL-EI over 2013:2017 does not fundamentally change the geography of SOL-EI accumulation over 2013:2017. Neither does subtracting IOP , as shown in Fig. A5. So we conclude that subtracting both CNS and IOP from absolute SOL-EI is an adequate method to uncover the interplay of processes (i.e., trends in air-sea flux and ocean heat transport divergence) that leads to the recent unabated SOL-EI accumulation (Fig. 4).

This approach readily reveals that regions which only experienced low positive SOL-EI accumulation under CNS (Fig. 5, top left) often show much increased warming in the recent period (Fig. 4, top panels). This is a general behavior found in all ocean basins, but the Eastern Pacific and tropical Pacific show outstanding rates of increased warming. This widespread maximum in SOL-EI accumulation in the Pacific dominates the zonal mean pattern in both Hemispheres (Fig. 3). In the North, it also corresponds to regions which have been highlighted as recent marine heatwave hotspots (Capotondi et al., 2024; Long et al., 2025; Jiang et al., in press).

https://doi.org/10.5194/egusphere-2026-4643
Preprint. Discussion started: 6 August 2026

Another key insight from the analysis of relative SOL-EI is that recent warming trends are mainly due to spatial redistribution of SOL-EI (bottom panels) rather than to a local increase in air-sea heat uptake (middle panels). For example, gradual accumulation of SOL-EI in the western Pacific revealed by CNS (Fig. 5, top left) yields increased divergence from this region leading to convergence in the eastern Pacific (Fig. 4, bottom panel).

Anomalies in heat transport convergence (Fig. 4, bottom) thus largely predict the sign and geography of recent changes in SOL-EI accumulation (Fig. 4, top). This is notably the case with increased warming in the tropical Indo-Pacific, and in the eastern Pacific as already discussed. In turn, increased SOL-EI divergence (Fig. 4, bottom) reduces warming rates within subtropical gyres, south of Equator in the Pacific, and in the tropical Atlantic (Fig. 4, top). The combined effect leads to a homogenization in cumulated warming rates when computed relative to 1980 (not shown).

The North Atlantic subpolar gyre (NA-SPG) stands out in that it shows SOL cooling in the recent period (Fig. 4, top and Fig. A5, bottom) which more than reverses the long-term trend of small SOL warming seen in the CNS (Fig. 5, top left). This is taking place despite increased heat uptake through the sea surface (Fig. 4, middle panel), owing to increased SOLEI transport divergence (bottom panel) that is found to be the leading order term. These findings corroborate a recent analysis of the North Atlantic subpolar warming hole which points to the AMOC as a key dynamical driver (Rahmstorf et al., 2026).

The North Atlantic subtropical gyre (NA-STG) on its poleward flank near the Gulf Stream and several locations along the Antarctic Circumpolar Current (ACC) also show significant compensation between increases in heat uptake and in heat transport divergence, with magnitudes in excess of $10W/m^2$. These regions, as was the case for NA-SPG, are characterized by mode water formation with winter mixed layers that reach 200m depth Speer and Forget (2013); Song and Forget (under review). But unlike for the NA-SPG, it is rather the increase in local heat uptake that dominates here and is only partly canceled out by increased heat transport divergence (Fig. 4). Another noteworthy feature of NA-STG is the contrast between the poleward side (SOLEI divergence) and the tropical side (SOLEI convergence), providing an illustration of how OHT can act to homogenize SOLEI accumulation (top panel).

The key to understanding regional SOL warming trends, which in themselves can be deceptive, thus lies in deciphering the often subtle imbalances between trends in regional heat uptake and in ocean heat transport divergence. Which process wins over the other depends on the region being considered. These findings highlight the importance for climate science of focusing on the estimation of complete heat budgets, as opposed to just the monitoring of ocean heat content changes. Closed heat budget estimates for the recent decades, constrained by observations, are required to attribute current warming trend patterns and better understand mechanisms that will control their evolution in the future.

Climate Variability

A complicating factor is that long-term trends can be obscured by climate variability at interannual to interdecadal time scales (Fig. 5-6). Wind-driven variability in the ocean circulation is generally the leading process, whereby ocean currents are modified by the action of anomalous wind stress, displacing upper ocean water masses, and air-sea heat fluxes react as a negative feedback (Frankignoul and Hasselmann, 1977; England et al., 2014; Forget and Ponte, 2015; Forget and Ferreira, 2019; Gu et al., 2024). The IOP pattern shown in the top right panel of Fig. 5 is viewed as a prime example. While it was derived simply

https://doi.org/10.5194/egusphere-2026-4643
Preprint. Discussion started: 6 August 2026

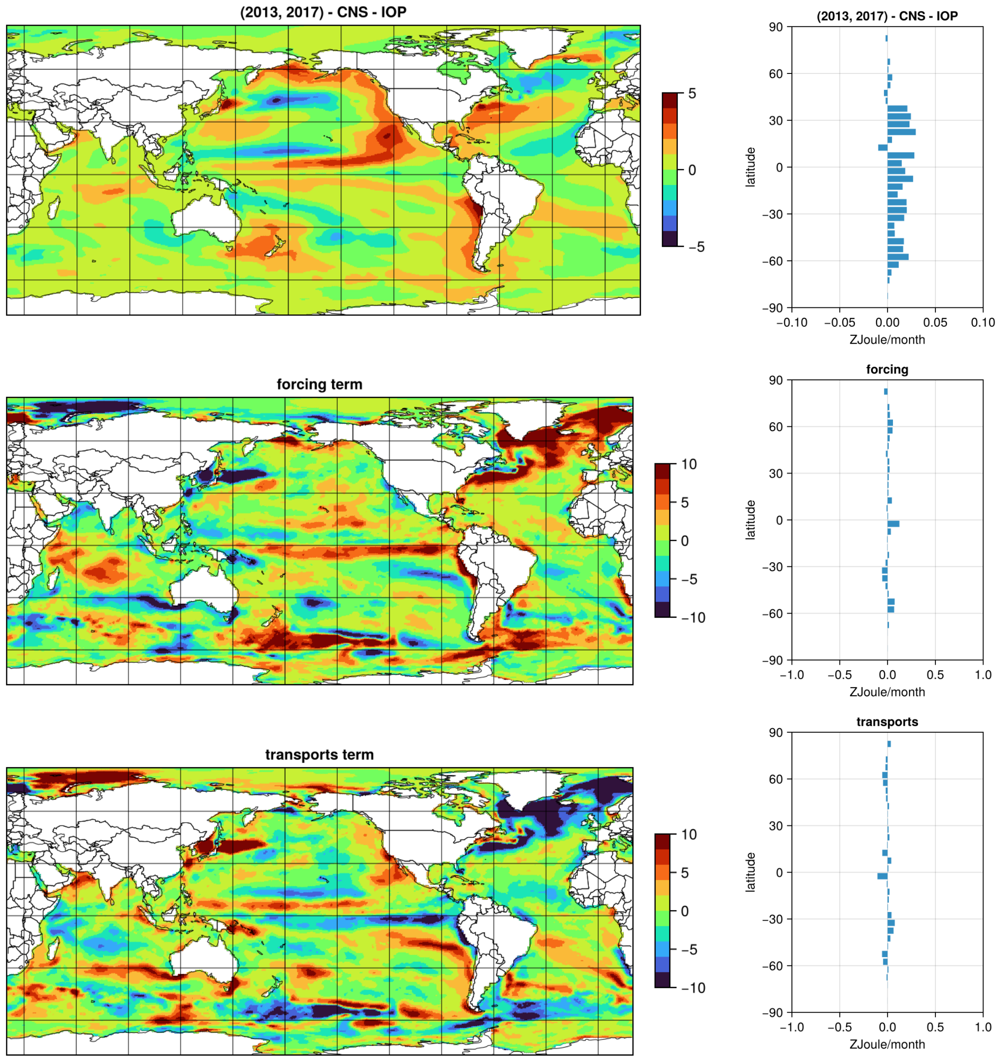

Figure 4. Relative SOL-EI as estimated in OCCA2.2A for 2013-2017. Relative SOL-EI is derived by subtracting the CNS and IOP contributions from absolute SOL-EI based on Eq. A10 (see sec A5 for detail). Left : in W/m2. Right : integrated over 5 degree latitude bands, in ZJoule/Month.

by imposing that spatial heterogeneity in SOL-EI is minimized over the CNS period, this pattern is reminiscent of the leading sea surface temperature mode of interdecadal variability known as the IPO (Salinger et al., 2001; Kosaka and Xie, 2013; Henley et al., 2015), showing large regions of significant anomalies outside the tropics. The corresponding IOP index mainly varies at interdecadal time scales. It is also noticeably distinct from the global SOL-EI index and the IPO index (Fig. 6, left panel).

The IOP geography is primarily controlled by ocean heat transport convergence (bottom right), which largely predicts the sign of ocean heat content anomalies (top right). However, the air-sea heat uptake term (bottom left) provides a negative

https://doi.org/10.5194/egusphere-2026-4643
Preprint. Discussion started: 6 August 2026

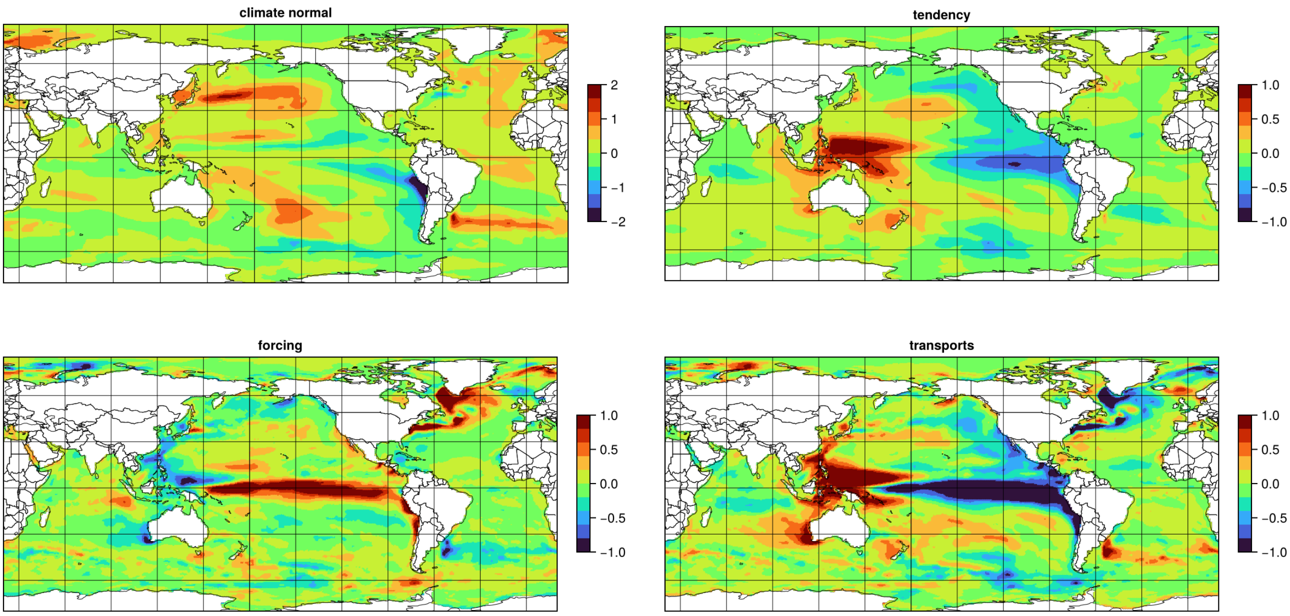

Figure 5. Top left : CLIMATE NORMAL STATE (OR CNS) as estimated in OCCA2.2A over 1985:2009 based on Eqs. A8-A9 (see section A5 for detail). Other panels : INTERDECADAL OSCILLATION PATTERN (OR IOP) pattern estimated jointly for the tendency term (top right), surface forcing (bottom left), and heat transport convergence (bottom right). Units: W/m2.

feedback that can compensate for (e.g., in the tropical) or even exceed (e.g., in the NA-SPG) the heat transport convergence term. An interesting result, which would deserve further study, is that air-sea heat flux feedbacks act in concert in NA-SPG and tropical Pacific as part of IOP , with the same sign in Fig. 6.

At interannual time scales, our analysis reveals a distinct pattern of tropical SOL-HB variability, which is characterized by compensating anomalies between the equatorial band and the northern tropics (Fig. 6, right panels). Here, interannual anomalies of ocean heat content and heat transport convergence are strongly correlated (Fig. 6, bottom right), indicating that heat transport tends to be the driving process, as one might expect (e.g., see Forget and Ferreira, 2019). Here, negative feedbacks via air-sea heat fluxes thus also significantly affect the SOL-EI budget from year to year (Fig. 6, bottom right).

Our general conclusion is that climate variability in SOL-EI and SOL-HB highlights compensating signals in the forcing and transport terms, which are so dominant that they are often larger than the residual heat content term signal (Figs. 4,5,6). The first order role played by negative feedbacks between air-sea heat exchange, reacting to OHT convergence anomalies, means that complete heat budget estimation should be viewed as an essential pre-requisite to making any robust inference of ocean heat content variability in terms of drivers, whether at interannual or interdecadal time scales.

https://doi.org/10.5194/egusphere-2026-4643
Preprint. Discussion started: 6 August 2026

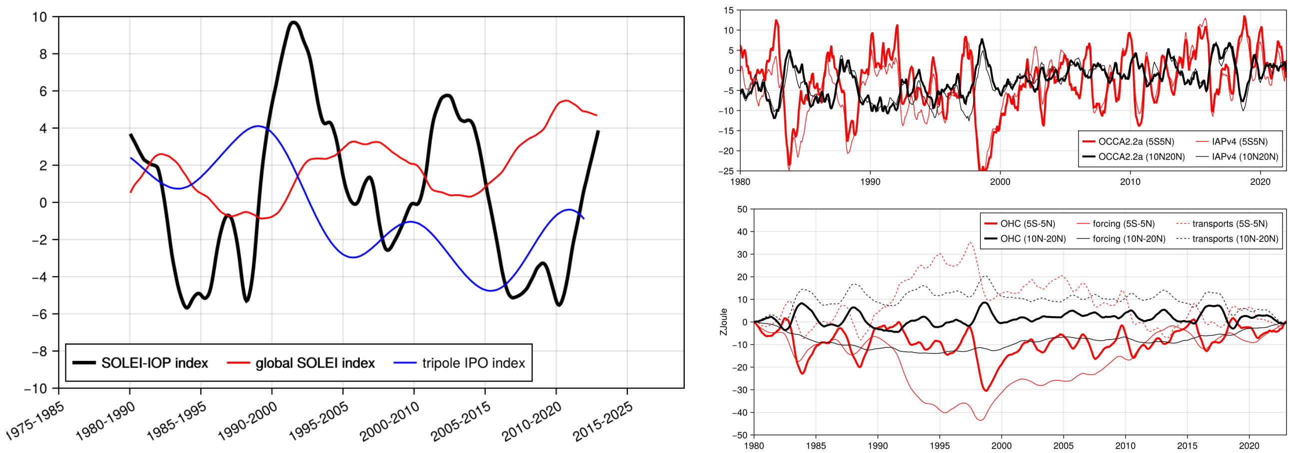

Figure 6. Left : non-dimensional index for IOP (Fig. 5) obtained by linear regression onto SOL-EI , along with the global SOL-EI index from Fig. 2, and the IPO index from Henley et al. (2015). The last two are multiplied by a factor of 10 to facilitate comparison. Top right : zonal mean ocean heat content anomaly, relative to the monthly 1980:2022 climatology, for the 5S-5N and 10N-20N latitude bands, in ZJoule. Bottom right : its breakdown in terms of surface forcing and heat surface convergence. Here the monthly heat budget climatology from 1980:2022 is subtracted before calculating annual means and integrating over time.

https://doi.org/10.5194/egusphere-2026-4643
Preprint. Discussion started: 6 August 2026

3 Conclusions

The innovative SOL-EI estimation framework introduced here – combining an operational definition of absolute and relative SOL-EI globally with a closed heat budget estimate plus an observation-based residual – provides a unified lens to attribute observed global trends, interdecadal variability, and regional patterns of near-surface ocean warming jointly. Focusing on the upper 200m Ocean layer – a useful proxy for climate feedbacks that respond to SST as well as for climate driven marine heatwaves – and on interdecadal time scales allows significant progress regarding key mechanisms. Applying this framework over 1980-2022 reveals the predominant role of ocean heat transport in driving interdecadal evolutions in the regional SOL-EI budget, including over the recent period.

Physical findings and implications

A major contribution of this study is the formulation of SOL-EI as a time-evolving equation for 10-year trends, rather than a single trend estimate for OHC. The resulting global SOL-EI index reveals rich interdecadal structure: it oscillates between near-zero values centered around 1993 and 2008 and elevated values of 30–60 ZJ/decade around 1987, 2001, and 2015. Two periods of low-SOL-EI , around 1993 and 2008, are linked to significant volcanic activity, which tends to reduce incoming shortwave radiation by injecting aerosol in the stratosphere and temporarily suppressed EEI (Church et al., 2005; Vernier et al., 2011; Fyfe et al., 2013; Medhaug et al., 2017; Dogar et al., 2020). The second period, known as *the hiatus*, was however affected by a broader combination of factors, including wind-driven heat redistribution and internal climate variability Kosaka and Xie (2013); England et al. (2014); Medhaug et al. (2017).

We show that the rate of SOL-EI accumulation has varied substantially over the past four decades in physically interpretable ways. Furthermore, the joint identification of an interdecadal oscillation pattern (SOL-EI -IOP) – resembling the IPO pattern but defined directly from SOL heat content estimates — establishes that a leading mode of climate variability leaves a coherent and analyzable imprint on SOL-EI geography. The 10-year running mean used to define SOL-EI reflects a deliberate choice (see also Minière et al., 2023) : it is long enough to filter out ENSO variability while short enough to track decadal shifts in accumulation rate that are physically and societally most relevant. Even so, a 40-year record is arguably too short to robustly separate interdecadal variability from the forced secular trend, underscoring the need to extend the analysis further backward as well as forward in time.

Perhaps our most consequential physical finding is that regional warming patterns in the SOL are generally controlled by the predominant influence of OHT convergence rather than by local air-sea heat uptake. This conclusion holds across ocean basins and time periods, and is corroborated by separate analyses of pathways and transports (Hersh et al., 2025; Song and Forget, under review, i; Jiang et al., in press; Forget et al., in prep.), as well as by independent reconstructions of historical OHT (Zanna et al., 2019). Heat accumulates where it is transported to, not simply where it enters the ocean. As a direct consequence, OHC change in the SOL, or SST change, viewed in isolation can be deceptive. It can even have the opposite sign to local air-sea exchange, as illustrated by the North Atlantic subpolar gyre.

https://doi.org/10.5194/egusphere-2026-4643
Preprint. Discussion started: 6 August 2026

The long term climatological balance between air-sea heat flux and OHT divergence typically is between two large terms, and must be removed before the much smaller imbalance signal becomes deciphered. The concept of relative SOL-EI , defined as an anomaly equation computed with respect to a carefully estimated climate normal state and with the IOP contribution removed, is a key analytical step needed to expose the regional interplay of Q and OHT trends. The practical implication of the predominant interplay of Q and OHT is that monitoring OHC trends alone cannot support robust mechanistic inference about the causes of regional warming at the sea surface.

An important feature of SOL-EI variability – at both interannual and interdecadal time scales – is the role of air-sea heat fluxes as a negative feedback responding to sea surface temperature anomalies. At interannual scales, we thus highlight tropical variability characterized by compensating anomalies between the equatorial band and northern tropics, where OHT convergence is the main driver and air-sea exchange induces significant damping. At interdecadal scales, SOL-EI -IOP interestingly reveals air-sea feedbacks that act in concert between the North Atlantic subpolar gyre and the tropical Pacific. These two regimes are distinct in spatial pattern and time scale yet share the same fundamental mechanism: OHT anomalies drive temperature changes to which the atmosphere responds via modified air-sea exchange, partially or fully offsetting the initial transport signal. Marine heatwave hotspots in the eastern and subtropical Pacific emerge naturally from this framework as regions where OHT convergence has persistently overcome damping by air-sea heat flux, leading to sustained SOL-EI accumulation (Capotondi et al., 2024; Long et al., 2025; Jiang et al., in press). SOL-EI convergence can thus play an important role in setting the background state that makes marine heatwaves more frequent and intense (Holbrook et al., 2019; Oliver et al., 2021). Anticipating and predicting such events will therefore require accurate closed heat budget estimates, rather than air-sea flux diagnostics or heat content monitoring alone.

Our results also support several forward-looking inferences, ranging from physically constrained predictions to more speculative conjectures. The rate of unabated SOL-EI accumulation estimated during the 2013–2017 peak, 30–60 ZJ/decade, is expected to continue in coming decades absent a major reduction in greenhouse gas forcing or exceptional volcanic perturbations. Aside from the global mean, the spatial structure of ongoing warming in the 0-200m layer carries predictive information. Subtropical warming already well established by 2007 is found reaching the equatorial band within approximately 15 years, based on zonal means (Fig. 3). This result suggests a rise of 0.5 K or more in subsurface tropical temperatures within the next 15 years based on the amount of additional warming that has taken place since 2007 in the subtropics. The 15 years time scale tracks with previous analysis of climate signal pathways from the subtropics to the equator via the ocean subsurface (Gu and Philander, 1997), which we suspect may also play a central role in IOP , through periodic injections of subtropical temperature anomalies into the equatorial thermocline , even though changes in ocean circulation pathways may introduce additional uncertainty. Given the role of tropical sea surface and subsurface temperatures in driving climate variability (Kosaka and Xie, 2013; Watanabe et al., 2024), tropical cyclone intensification and atmospheric river activity, this prospect is particularly concerning. To firm up this conjecture, targeted Lagrangian analyses of time scales and pathways in OCCA2 or climate models would seem useful (Gu and Philander, 1997; Rousselet et al., 2021; Hersh et al., 2025). We also conjecture, more speculatively, that the North Atlantic subtropical gyre may serve as a leading indicator for what is yet to come in the Pacific. The same SOL-EI convergence dynamics appear to govern both basins, but the larger size of the Pacific implies a longer gyre recirculation timescale,

https://doi.org/10.5194/egusphere-2026-4643
Preprint. Discussion started: 6 August 2026

delaying EEI saturation in the subtropical gyre interior – the Atlantic may, in effect, be ahead of the Pacific on a comparable but longer trajectory.

Methodological outlook

The sunlit ocean layer, bounded at 200 m depth, is introduced here as a physically motivated concept rather than another ad hoc depth level. Unlike other choices of depth horizon commonly found in the literature (Zanna et al., 2019; Bagnell and DeVries, 2021; Minière et al., 2023; Li et al., 2023b; Wu et al., 2025) — surface to some mixed layer depth estimate, 0–300 m, 0–700 m, or 0–2000 m — the choice of 200 m is rooted in the exponential decay of downwelling solar radiation with depth that provides a fundamental theoretical underpinning (Fig. A11). Below this depth direct radiative forcing is negligible. Two hundred meter depth furthermore defines a fixed geometric volume that is more tractable for closing heat budgets than a seasonally and spatially varying mixed layer depth, and it provides a more informative proxy for sea surface temperature than thicker layers do. Finally, 200m is also frequently used to delimit the euphotic layer where biological impacts of warming are concentrated — from shifts in phytoplankton phenology to coral bleaching events — making SOL the natural unit for assessing the consequences of EEI accumulation on marine ecosystems and the human communities that depend on them.

A key methodological lesson of this study is that closed heat budget estimates constrained by data and theory are indispensable for a mechanistic interpretation of SOL-EI . OCCA2 and ECCO4 represent the current state of the art in this regard, and arguably the only observational state estimates that presently enforce strict budget closure requirements. They remain insufficient, however, to fully characterize uncertainties in the Q and OHT terms on the right-hand side of the SOL-EI equation (e.g., see Forget and Ferreira, 2019; Liu et al., 2020). Within the OCCA2 framework, a tractable path toward improvement lies in further reducing the, already small, residual non-conservative budget terms by further optimizing model parameters via the ECCO4 adjoint machinery (Forget et al., 2015b; Forget and Ponte, 2015; Forget et al., 2015a).

The architecture of the OCCA2 family of estimates is furthermore designed to be extensible: just as Argo profiles are used to derive the $\delta\mathbb{T}_{O2.2b\rightarrow O2.2d}$ adjustment over 2004–2022, any gridded OHC product can in principle be incorporated as an additional family member, as a non-conservative adjustment term. Differences between IAPV4 and OCCA2.2B can thus be used to define a pre-Argo branch of OCCA2, and extend the budget uncertainty framework throughout 1980-2003. This extensibility means that improvements in any upstream observational product will translate directly into improved SOL-EI estimates within the OCCA2 framework.

Since all three terms in SOL-EI are typically of comparable magnitude, and the OHC term is often smaller than the other two, precisely monitoring OHC alone is insufficient to assign drivers with certainty. Knowing OHC anomalies even more accurately from observations could not resolve this issue unless either Q or OHT convergence were negligible or perfectly known. Our results show neither term is generally negligible, which means that reducing uncertainties individually in Q and OHT must take priority. While broad agreement between ECCO's OHTand various gridded Q estimates has been demonstrated for the time-mean balance (Forget and Ferreira, 2019), much remains to be done for time-variations. An ensemble of observational reanalyses, based on diverse model configurations and parameter choices, is needed to address structural and parametric uncertainty in a statistically meaningful way (Forget et al., in prep.).

https://doi.org/10.5194/egusphere-2026-4643
Preprint. Discussion started: 6 August 2026

Advancing SOL-EI estimation will require targeted progress on at least two observational fronts. The first is ocean heat transport, currently the most poorly constrained term in the SOL-EI equation when it comes to observations. Argo profiles yields indirect transport information (Forget et al., 2008a, b, ,and others) and satellite data already assimilated in ECCO can partially bridge these gaps (Forget and Ponte, 2015; Meyssignac et al., 2024). However, marginal seas remain largely undersampled by the global observing system, and are likely a substantial gap in our ability to constrain the SOL-EI equation globally. Worldwide data sparsity before Argo (i.e. before 2004) also makes the early part of the record more uncertain (including the 1993 minimum in SOL-EI). The second front is air-sea heat exchange. Latent and sensible heat fluxes over the open ocean remain particularly difficult to estimate accurately from either in situ measurements or atmospheric reanalyses, and their regional biases can propagate into SOL-EI budget residuals, limiting our ability to close the observational budget and attribute warming to processes with certainty.

The 40-year record underpinning our analysis also remains too short to fully characterize interdecadal variability or to cleanly separate it from the forced secular trend. Over this period, the SOL-EI -IOP index goes through only 3 maxima and 3 minima, the global SOL-EI index only experiences two of each, and neither index seems to coincide with the tripolar IPO index very well (Henley et al., 2015). Extending OCCA2 further back in time — by combining the optimized ECCO4 model parameters with ERA5 or the forthcoming ERA6 reanalysis — is both technically feasible and viewed as a high priority, particularly given that pre-1980 OHT reconstructions show important low-frequency variability (Zanna et al., 2019). The encouraging agreement between OCCA2 and IAPv4 over the pre-Argo period provides confidence that such an extension would continue yielding physically insightful results. More broadly, the continued expansion and diversification of the global ocean observing system — including Argo, deep Argo, biogeochemical sensors, and satellite data — remains essential. The ability to monitor SOL-EI and its drivers in near real time, and to reduce uncertainties progressively, will be crucial to anticipate and predict the potentially catastrophic environmental consequences of accelerating SOL-EI accumulation in the decades ahead.

Code and data availability. Upon publication of the final revised paper, the minimal dataset necessary to interpret, replicate, and build upon the findings reported here will be placed in a publicly available repository. Re-running OCCA2.2A is made easy by the ClimateModels.jl and MITgcmTools.jl open-source libraries. ArgoData.jl provides the Argo data and method used to map anomalies. Access to ECCO4 and OCCA2 estimates, and analyses in this paper, can be repreduced using the Climatology.jl and Dataverse.jl open-source libraries.

Appendix A: Methods

OCCA2 is a family of solutions designed to jointly estimate SOL-EI and quantify its uncertainty. Its core member, OCCA2.2a, provides a closed heat budget estimate for 1980-2022. OCCA2.2b adjusts the monthly mean climatology to match ECCO4, while OCCA2.2c and OCCA2.2d incorporate progressively closer fits to Argo observations. The difference between OCCA2.2d and OCCA2.2c serves as a concrete, observation-based uncertainty estimate for the closed heat budget.

The estimation process starts from the ECCO4 ocean reanalysis, which provides a closed heat budget estimate for the global ocean constrained by most relevant observations (Forget et al., 2015b; ECCO Consortium et al., 2021). Crucially, ECCO4's SOL-HB resolves the air-sea flux terms and ocean transport terms that are often missing in other observational estimates (Forget and Ferreira, 2019; Meyssignac et al., 2024). We extend ECCO4 to the 1980-2022 period by combining the optimized ECCO4 model parameters with the ERA5 atmospheric reanalysis (Hersbach et al., 2020). To quantify uncertainty, we then 1. map out residual differences to Argo temperature profile collections from 2004 onwards (Roemmich et al., 2019), and 2. compare OCCA2 with another observational estimate of ocean heat content over the full 1980-2022 period (Cheng et al., 2024b).

A1 Context

OCCA stands for *OCean Comprehensible Atlas* (Forget, 2010). As in ECCO state estimates (Forget et al., 2015a), OCCA is based on adjoint-optimized solutions of the MIT general circulation model (MITGCM), which provides closed heat and freshwater budgets and gridded transports across space and time (Forget, 2010; Forget and Ponte, 2015; Forget and Ferreira, 2019). But unlike in ECCO estimates, we allow for relatively small deviations from strict budget closure in OCCA, to enable a slightly closer fit to Argo (Fig. A8, section A8 and reference Forget, 2010).

Compared to other climatologies based on Argo like WOA-2023 Reagan et al. (2024) or IAPV4 Cheng et al. (2024b), on the other end, OCCA state estimates greatly increase interpretability by providing full heat and freshwater budgets that resolve air-sea fluxes and all ocean transport terms. In OCCA1, this goal was achieved by optimizing consecutive MITGCM solutions, of 16 months each, and making a gradual transition during the four-month overlap. This approach led both to a closer fit to Argo than in ECCO3, and to a greater interpretability than with optimal interpolation (Forget, 2010).

Following OCCA1, a major step forward was taken in ECCO4 – internal ocean model parameter optimization was added to effectively reduce spurious model drifts and improve the fit to Argo while maintaining strict budget closure (Forget et al., 2015a, b). This enables a novel strategy in OCCA2, where we start by simply extending ECCO4-RE2 (Release 2) from 1992-2011 to 1980-2022 (OCCA2.2A). Longer analysis periods are a major priority for the reanalysis user community (Yang et al., 2024) and generally useful to improve the estimation of statistics and separate out climate variability (e.g. ENSO oscillations, volcanic eruptions, IPO) from long-term trends and global climate change (Wu et al., 2019; Dogar et al., 2020).

A2 Closed Budget Estimates

The OCCA2.2A surface forcing is created by (1) replacing the ECCO4-RE2 forcing fields with ERA5 forcing fields, (2) computing a monthly climatology of the difference over 1992-2011, and (3) adding it onto ERA5 every year over 1960-2022.

https://doi.org/10.5194/egusphere-2026-4643
Preprint. Discussion started: 6 August 2026

Optimized ocean mixing parameters are simply taken from ECCO4-RE2 and reused in OCCA2.2A without modification (Forget et al., 2015b). This straightforward method transfers data-constrained elements of ECCO4 to the new simulation, and reduces spurious drifts in climatology. While OCCA2.2A derives its skill partly from how Argo data was used to constrain transport parameterizations in ECCO4-RE2 (Forget and Ponte, 2015), we note that Argo data collected after 2011 is completely independent from OCCA2.2A.

Initial conditions for OCCA2.2A (1980-present) were derived via a spin-up carried out by intergrating the model over 1960-1980. This initial integration is designed to adjust ECCO4-RE2's initial state to 1980 conditions. While reanalyses like ERA5 do not reliably enforce volume conservation, we adopt a simple approach to treat spurious global mean imbalance in Earth's water cycle. Hence in OCCA2.2A we use an MITGCM option that keeps the global ocean mass constant (seawater plus ice), by adding a globally uniform correction at each model time step that cancels out the global water flux across the surface. This global adjustment is very small compared with local evaporation and precipitation rates, and therefore has virtually no impact on ocean dynamics or on the fit to Argo (Forget et al., 2015a). It simply allows us to separate out issues and focus on the heat budget.

Time series of temperature anomalies from OCCA2.2A over 1980-2022 are depicted in Figs. 1,2,3,6. These are unchanged in the OCCA2.2B estimate, which is exactly the same as OCCA2.2A expect that the monthly mean seasonal cycle is adjusted to match ECCO4-RE2 over the overlapping 1992-2011 period (Eq. A1). The result is a closed heat budget estimate, formed by linear combination of two closed heat budget estimates, that more closely fits Argo data (see section A8, Fig. A8).

$$\mathbb{T}_{OCCA2.2b} \quad = \quad \mathbb{T}^{cycle}_{ECCO4.2} + \delta\mathbb{T}^{inter}_{OCCA2.2a} \tag{A1}$$

A3 Heat Budget Calculations

Heat and volume budgets (extensive properties, ΔH and ΔV) are first derived from the monthly model output for OCCA2.2A. The equations for ΔH and ΔV are closed to machine precision within MITgcm, and outputting results at double precision allows us to preserve budget closure. Calculations are carried out between the ocean free surface (below seaice when it exists) and the sea floor. Gridded heat and volume budget outputs are then combined to form the tendency equation for temperature (intensive property, T) at constant grid cell volume as explained in Forget et al. (2015a); Forget and Ferreira (2019).

For any given time interval (t_0,t_1) and grid cell (i,j,k), this can be written as $\Delta T = \left(\frac{\Delta H}{\rho c_p} - T_0 \Delta V\right)/V_1$, where ρ is the density, c_p is the specific heat capacity, and V_0 is volume at time t_0. This treatment is applied separately to the transport and forcing convergence terms, grid point by grid point, to obtain the closed equation for $\frac{\partial T}{\partial t}(i,j,k,t)$. The interplay of processes that regulate temperature anomalies is obtained by integrating the temperature tendency equation through time (Eqs. A2-A4). Results can then easily be presented relative to a seasonal mean climatology (e.g., Fig. A1,A6,A7) and/or by integrating over constant volume grids (Figs. A2-A3).

To interpret the global mean temperature equation in terms of vertical flux, a time-invariant offset (0.2 W/m2) is calculated by integrating the transport tendency term globally on the fixed volume grid ($V_0(i,j,k)$. In Fig. 2, this offset is subtracted from

https://doi.org/10.5194/egusphere-2026-4643
Preprint. Discussion started: 6 August 2026

the net vertical heat flux profile, consistently across the surface forcing and transport terms. Indeed, this offset derives from converting budgets to a constant volume framework and cannot simply be interpreted as a net vertical heat flux.

$$\mathbb{T}'_{t0}(t) = \int_{t0}^{t} \frac{\partial \mathbb{T}}{\partial t} dt \tag{A2}$$

$$\mathbb{T}'_{t0}(t) = \text{FORCING}_{t0}(t) + \text{TRANSPORTS}_{t0}(t) \tag{A3}$$

$$\overline{\mathbb{G}}^{t0,t1} = \frac{1}{t1 - t0} \mathbb{T}'_{t0}(t1) \tag{A4}$$

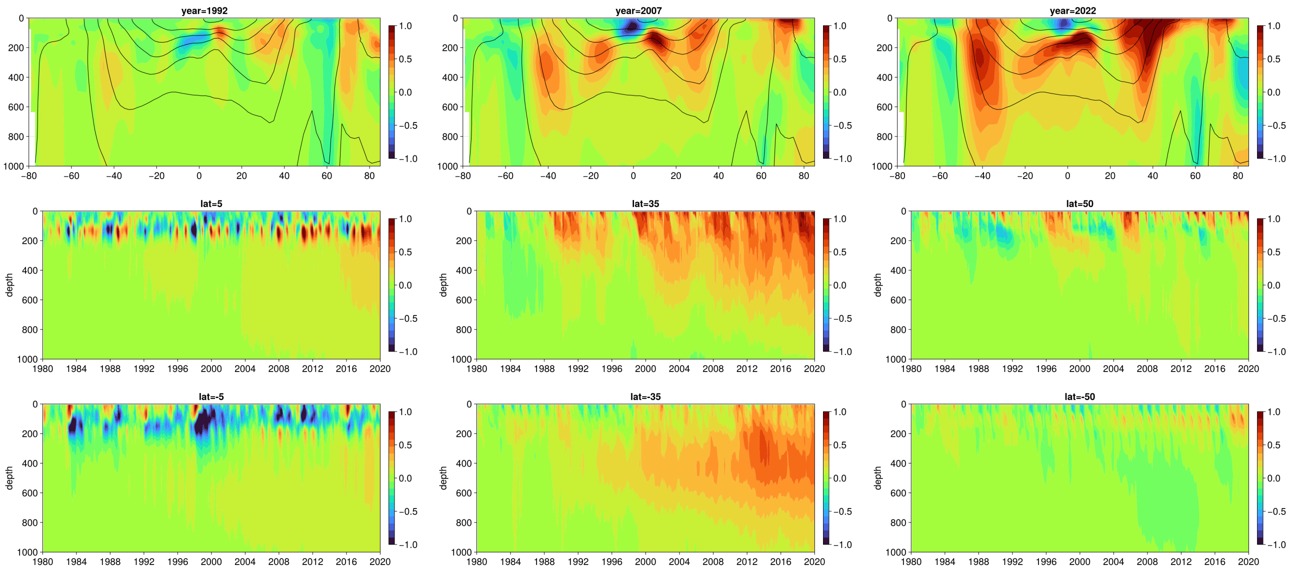

Figure A1. Zonal mean temperature anomalies relative to 1980-1982 climatology in OCCA2.2A-OCCA2.2B-OCCA2.2C. Top : 1992 (left), 2005 (middle), and 2022 (right). Middle : 5N, 35N, and 50N. Bottom : 5S, 35S, and 50S. Units: degree Celsius.

A4 Defining Ocean Energy Imbalance

Eqs. A2-A4 provide a window into ocean energy imbalance over period $t0, t1$, which can then be integrated over any ocean volume to derive budgets of ocean heat content change. Fig A2 shows examples for the zonally integrated SOL-HB over two different periods. The SOL-HB anomaly computed between these two periods is mapped out in Fig A3.

A challenge with interpreting calculations like these is that they tend to alias short term variability, since Eq. A4 amounts the difference between two ocean snapshots (respectively, at times $t1$ and $t0$). To circumvent this difficulty and better focus on decadal and longer time scales, we therefore substitute the time derivative from Eq. A2 with its ten-year running mean in Eq. A5.

The same ten-year running mean $\mathcal{H}$ is applied to the FORCING and TRANSPORTS terms, within the time integral, leading to Eq. A6. The temporal smoothing of the temperature tendency equation naturally carries over to time integrated results e.g. in

https://doi.org/10.5194/egusphere-2026-4643
Preprint. Discussion started: 6 August 2026

Fig. 2 (top panel) and Fig. 3 (compared with Fig. A1). Hence, Eq. A7 provides the definition of ocean energy imbalance used in this paper.

$$\mathbb{T}^{\mathcal{H}}_{t0}(t) = \int_{t0}^{t} \mathcal{H}(\frac{\partial \mathbb{T}}{\partial t})dt \tag{A5}$$

$$\mathbb{T}^{\mathcal{H}}_{t0}(t) = \text{FORCING}^{\mathcal{H}}_{t0}(t) + \text{TRANSPORTS}^{\mathcal{H}}_{t0}(t) \tag{A6}$$

$$\overline{\mathbb{H}}^{t0,t1} = \frac{1}{t1 - t0}\mathbb{T}^{\mathcal{H}}_{t0}(t1) \tag{A7}$$

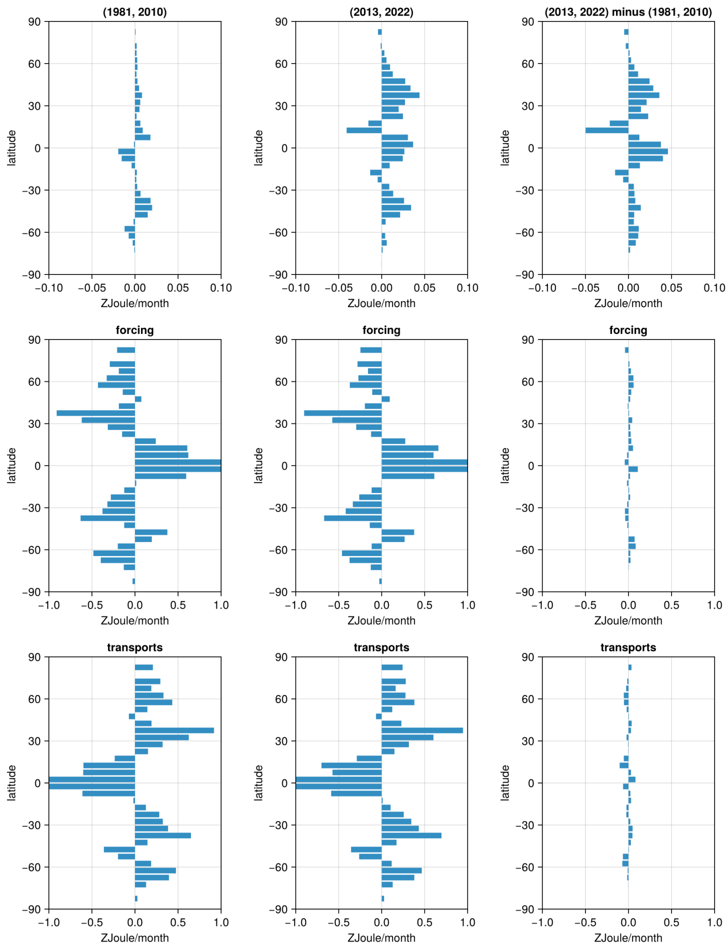

Figure A2. SOL-HB budget in OCCA2.2A for 1981:2010 (left), 2013:2022 (middle), and the difference (right) based on Eq. A3. Units : ZJoule/month.

https://doi.org/10.5194/egusphere-2026-4643
Preprint. Discussion started: 6 August 2026

A5 Defining Relative Ocean EI

Comparing SOL-HB over two different periods (Fig. A2) immediately reveals that on a regional basis interdecadal changes (right panel) are generally small compared with the time-invariant balance of air-sea flux and ocean heat transport divergence Forget and Ferreira (2019). It is therefore useful to analyze SOL-EI relative to a reference state that captures the time-invariant first-order regional balance in SOL-HB , which would be present even in the absence of global warming.

A simple but suboptimal approach would be to choose a long-term average of SOL-HB , as done in Fig. A3. However, this approach tends to be particularly prone to aliasing global patterns of climate variability at the end points of the SOL-HB integration (Eq. A2). Even a twenty-five-year SOL-HB would thus capture a specific phase of the Interdecadal Pacific Oscillation (IPO Salinger et al., 2001; Kosaka and Xie, 2013; Henley et al., 2015) and other climate variability modes.

To mitigate this issue, we construct instead a long term average of SOL-EI , which is named *climate normal* SOL-EI (or CNS). To make CNS as neutral as possible with regard to the phase of leading climate modes, we derive it as a weighed average of SOL-EI over 1985 to 2009. This twenty five year period was chosen, taking advantage of the first three decades of OCCA2.2A, to average over periods of both low and high absolute SOL-EI (Fig. 2, bottom).

Furthermore, we modulate the time-averaging weights w_i in Eq. A8 under the constraint of minimizing Eq. A9, where the first term penalizes spatial heterogeneity while the other two penalize departures from the $\mathbb{H}_0(\mathbf{1})$ first guess. Regularization factors a and b are both set to 0.1. The chosen approach presents the additional benefit that applying the optimized $\boldsymbol{w}$ to the FORCING and TRANSPORTS terms readily preserves strict budget conservation.

$$\mathbb{H}_0(\boldsymbol{w}) = \sum_i [\frac{w_i}{\sum_j w_j} h_i] \tag{A8}$$

$$J(\boldsymbol{w}) = \sum_{x,y} [\mathbb{H}(\boldsymbol{w})^2] + a \times \sum_i [(w_i - 1)^2] + b \times (\sum_{x,y} [\mathbb{H}(\boldsymbol{w}) - \mathbb{H}_0(\mathbf{1})])^2 \tag{A9}$$

The optimized CNS estimate, $\widehat{\mathbb{H}}_0$, is very similar to $\mathbb{H}_0(\mathbf{1})$ over most of the global ocean (Fig. A4). However, as one may have anticipated, optimizing $\boldsymbol{w}$ based on Eq. A9 filters out an IPO-like pattern in $\mathbb{H}_0(\mathbf{1})$ (middle panel of Fig. A4). We can then verify that the difference, $\widehat{\mathbb{H}}_m = \widehat{\mathbb{H}}_0 - \mathbb{H}_0(\mathbf{1})$, identifies an INTERDECADAL OSCILLATION PATTERN (OR IOP) by regressing $\widehat{\mathbb{H}}_m$ onto $\mathbb{T}^{\mathcal{H}}_{t0}(t)$ and plotting the resulting $\alpha(t)$ index (Fig. 5, left panel). While IOP is reminiscent of the IPO pattern, it is defined directly based on SOL heat content estimates.

In conclusion, Eqs.A8-A9 define not only CNS but also, jointly, the IOP index and geographical pattern (Figs. 5,6). Subtracting both CNS and IOP from Eqs. A5-A7 leads to our specification of relative SOL-EI as

$$\overline{\mathbb{H}}^{t0,t1} - \overline{\alpha}^{t0,t1} \times \widehat{\mathbb{H}}_m - \widehat{\mathbb{H}}_0 \tag{A10}$$

for the SOL-EI accumulation term, and similarly for FORCING$^{\mathcal{H}}_{t0}(t)$ and TRANSPORTS$^{\mathcal{H}}_{t0}(t)$.

https://doi.org/10.5194/egusphere-2026-4643
Preprint. Discussion started: 6 August 2026

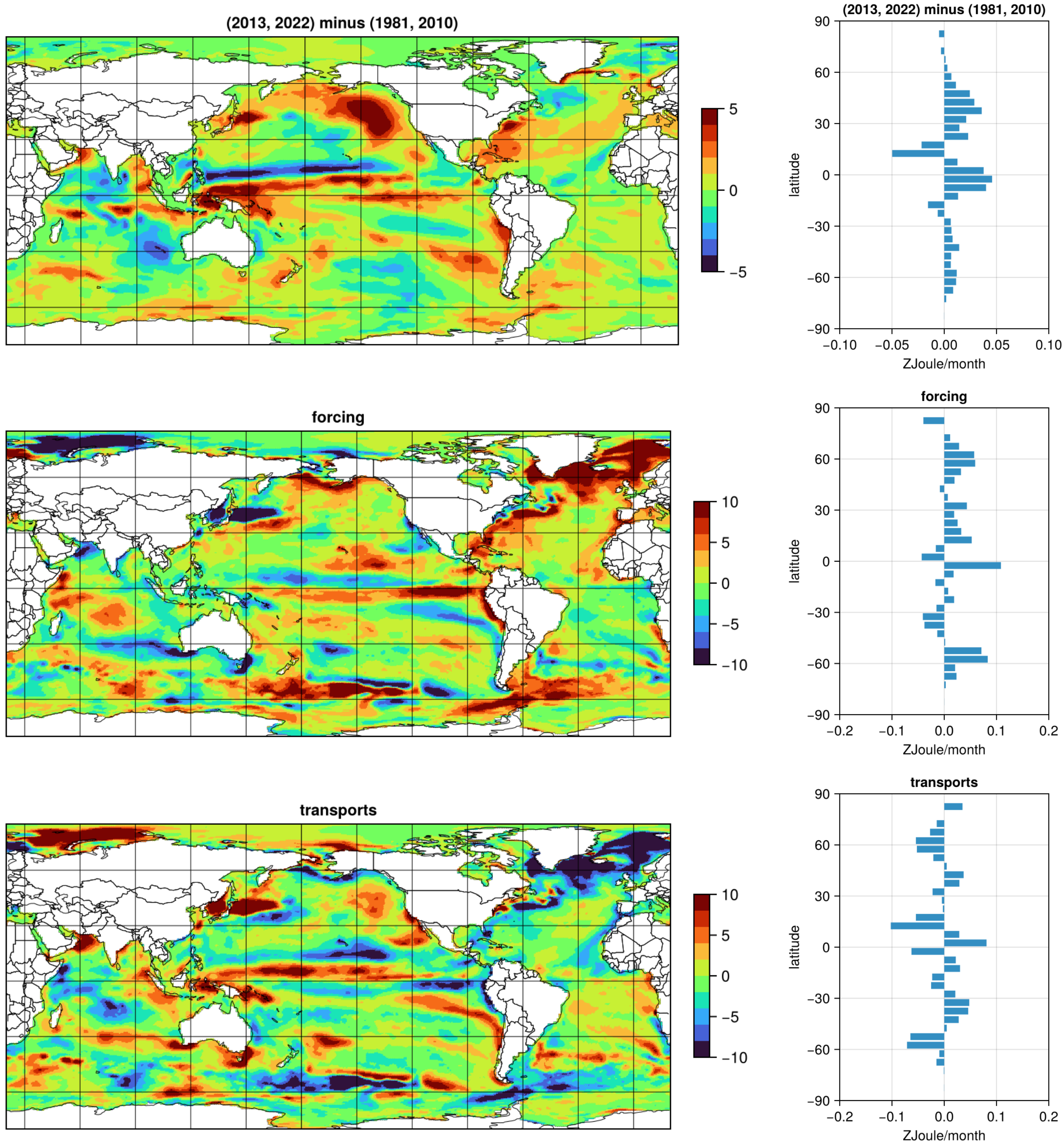

Figure A3. Difference in SOL heat budget climatology computed between 2013-2022 and 1981:2010 in OCCA2.2A based on Eq. A3. The closed heat budget estimate (top) is the sum of EEI uptake through the sea surface (middle) and ocean EI transport convergence between the surface and 200m depth (bottom). Units: W/m2. Right panels : integrated over 5 degree latitude bands, in ZJoule/Month.

https://doi.org/10.5194/egusphere-2026-4643
Preprint. Discussion started: 6 August 2026

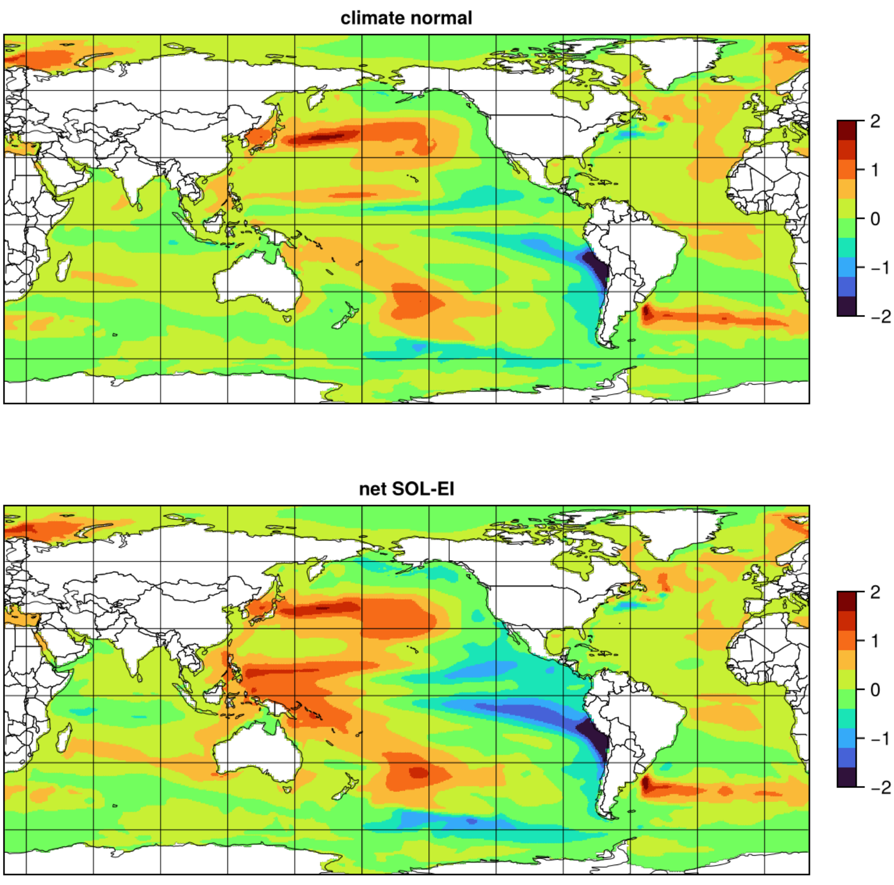

Figure A4. Climate normal SOL-EI (top) derived from OCCA2.2A over 1985:2009 by optimizing Eq, A9, and the corresponding time average for absolute SOL-EI (bottom). Units: W/m2.

https://doi.org/10.5194/egusphere-2026-4643
Preprint. Discussion started: 6 August 2026

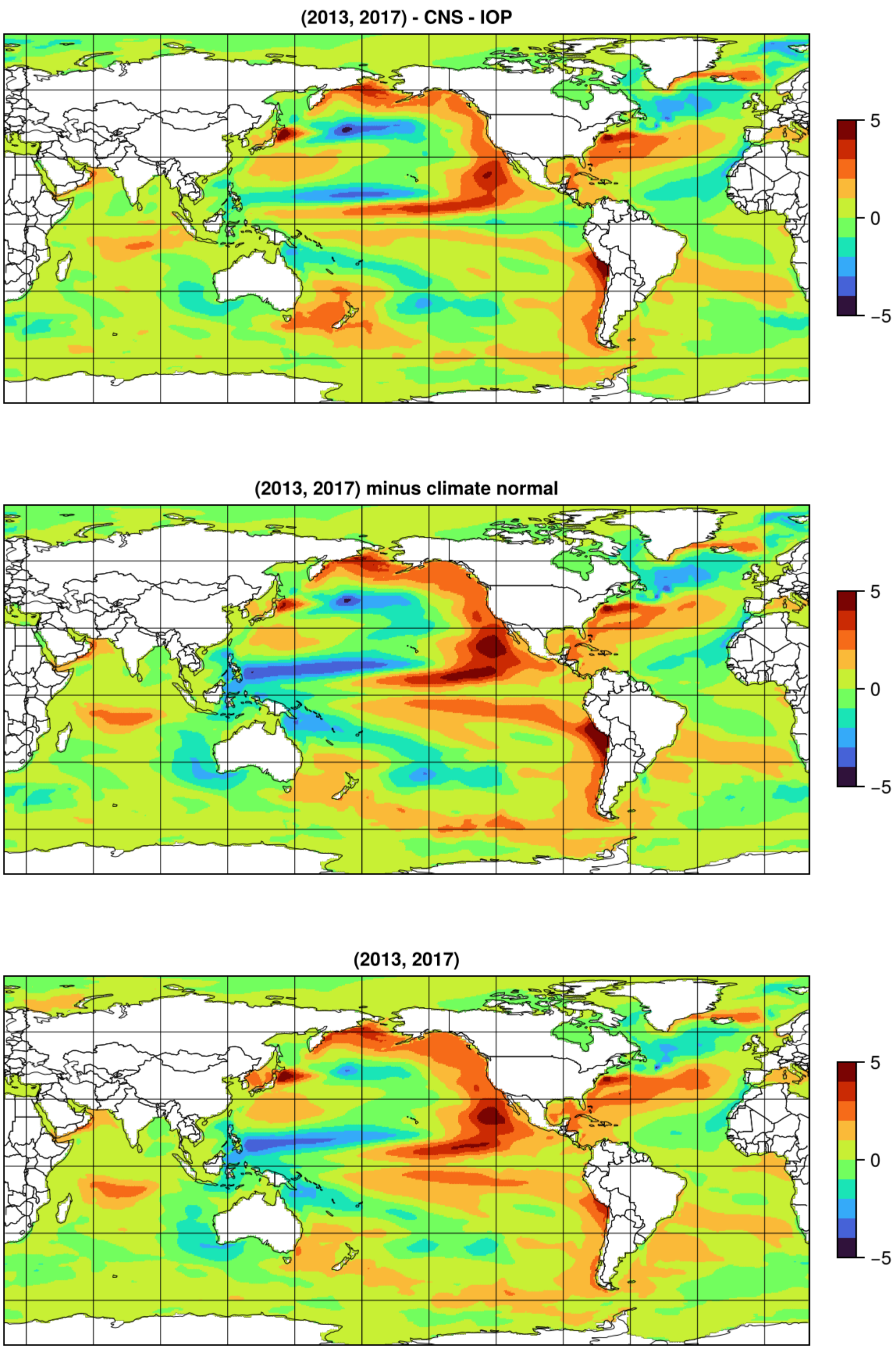

Figure A5. SOL-EI anomaly estimated by integrating Ocean Energy Imbalance in OCCA2.2A over 2013-2017 (bottom panel), then subtracting the climate normal estimated over 1985-2009 (middle panel), and then subtracting the INTERDECADAL OSCILLATION PATTERN (OR IOP) estimated over 1985-2009 (top panel). Units: W/m2.

https://doi.org/10.5194/egusphere-2026-4643
Preprint. Discussion started: 6 August 2026

A6 Temperature Uncertainty Quantification

445 To derive uncertainty estimates for the heat budget equation (section A9), we start by calculating pointwise differences between Argo profiles and OCCA2.2B, which we then map on the global grid (section A7). Pointwise differences are calculated in two stages. First, a mean monthly difference, $\delta\mathbb{T}^{cycle}_{O2.2b\rightarrow O2.2c}$, is computed over 2004-2022, and added to OCCA2.2B to obtain OCCA2.2C. Second, a time variable monthly adjustment, $\delta\mathbb{T}^{inter}_{O2.2c\rightarrow O2.2}$, is computed from the remaining difference between Argo profiles and OCCA2.2C profiles (Figs. A6). The final estimate, OCCA2.2D , can be expressed as

450 $$\mathbb{T}_{OCCA2.2d} \quad = \quad \mathbb{T}_{OCCA2.2b} + \delta\mathbb{T}^{cycle}_{O2.2b\rightarrow O2.2c} + \delta\mathbb{T}^{inter}_{O2.2c\rightarrow O2.2} \tag{A11}$$

where $\delta\mathbb{T}$ denotes an anomaly in temperature, $cycle$ a mean monthly seasonal cycle, and $inter$ a time series of interannual departure from a mean seasonal cycle. The last two terms are computed over the 2004-2022 period that Argo resolves, using the mapping method described in section A7. Each added term leads to an increasingly close fit to Argo as expected (section A8).

Importantly, the seasonal-mean adjustments from OCCA2.2A to OCCA2.2C do not contribute to the relative SOL-EI equa-
455 tion. Only $\delta\mathbb{T}^{inter}_{O2.2c\rightarrow O2.2d}$ contributes to the ocean evolution and trends discussed in this paper (Figs. 1-2,A6,A7,A9). It can be viewed as an additional, non-conservative heat budget term required to track Argo profiles optimally (section A8), or equivalently as an estimate of uncertainty for the closed heat budget estimate (section A9).

Before the Argo period (i.e., pre-2004), data sparsity prevents such direct uncertainty quantification from profile data. To extent our assessment of uncertainty to 1980-2022 (Figs 2, 5, A10), we instead leverage an ocean temperature reanalysis called
460 IAPV4 (Cheng et al., 2024b), which uses historical data to reconstruct the pre-Argo period. While uncertainties in IAPV4 are not fully known, differences between IAPV4 and OCCA2.2B provides a measure of uncertainty for both products.

More generally, we note that the difference between any gridded OHC product and OCCA2.2b can be treated as an analogous adjustment term within the OCCA2 framework (Eq. A11), extending the same uncertainty quantification architecture used with Argo to the pre-Argo period and to alternative observational products.

465 ### A7 Geospatial Argo Statistics

The last two terms in Eq. A11 are based on geo-spatial mapping of difference between Argo profile collections and OCCA2 solutions. These contributions are analogous to the result of an objective mapping of Argo temperature anomalies computed from a climatological-mean seasonal atlas, as done in IAPV4 for example. In OCCA2 though, this non-conservative SOL-HB term is a small residual compared with the observed trends, because the prior to the objective mapping is an already
470 accurate and complete map of the time-evolving monthly SOL-HB (Forget and Ponte, 2015). By reducing the magnitude of non-conservative terms in this fashion, OCCA2 enhances the interpretability of gridded ocean temperature estimates.

To map out the differences between OCCA2 solutions and Argo, we use a method that is an update to the objective mapping used in OCCA1 Forget (2010); Forget and Wunsch (2007). It proceeds in two steps : 1. sample average pointwise misfits over grid boxes of decreasing size, and 2. compute a weighted average of these sample averages over the OCCA2/ECCO4 grid

https://doi.org/10.5194/egusphere-2026-4643
Preprint. Discussion started: 6 August 2026

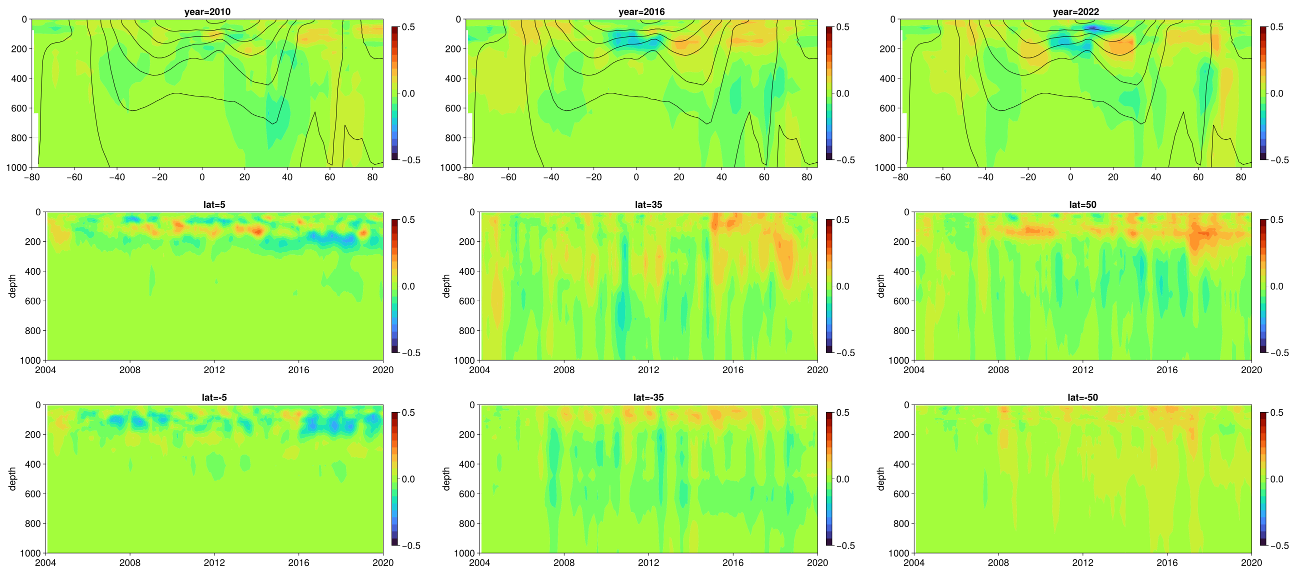

Figure A6. Zonal mean temperature anomalies from OCCA2.2D minus OCCA2.2A relative to the 2004-2006 climatology. Units: degree Celsius. Top : 2010 (left), 2016 (middle), and 2022 (right). Middle : 5N, 35N, and 50N. Bottom : 5S, 35S, and 50S.

(Forget et al., 2015a). The code is open source, available on GITHUB.COM via the ARGODATA.JL software package, and will be further documented in a separate publication (in prep).

The starting point of our workflow is a copy of the Argo archive that downloaded from the Global Data Assembly Center on April 15th, 2023. Argo profiles are first converted from the native Argo format to the MITPROF standard profile format used in ECCO4 (Forget, 2010; Forget et al., 2015a). To this end, the ARGODATA.JL open-source library interpolates all Argo profiles to standard depth levels, and associates them with uncertainty profiles that define the cost function in Fig. A8.

https://doi.org/10.5194/egusphere-2026-4643
Preprint. Discussion started: 6 August 2026

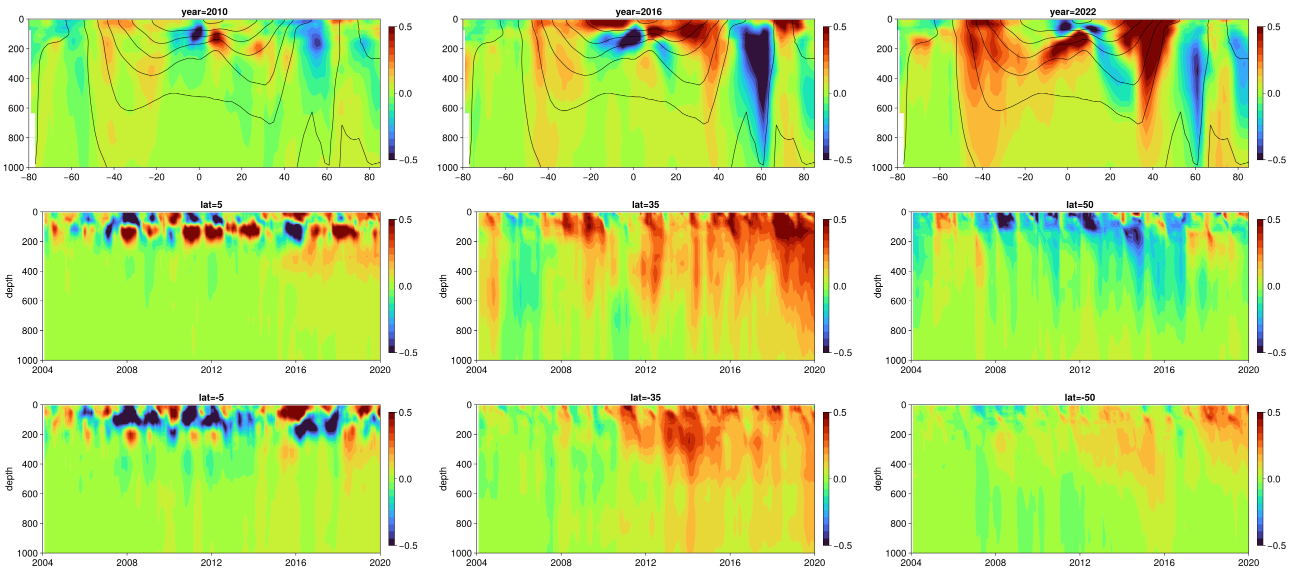

Figure A7. Zonal mean temperature anomalies relative to 2004-2006 climatology in OCCA2.2A-OCCA2.2B-OCCA2.2C. Units: degree Celsius. Top : 2010 (left), 2016 (middle), and 2022 (right). Middle : 5N, 35N, and 50N. Bottom : 5S, 35S, and 50S.

https://doi.org/10.5194/egusphere-2026-4643
Preprint. Discussion started: 6 August 2026

A8 Fit to Argo Profiles

To measure the agreement between ocean profile collections and climatology estimates, it is important to use a normalized cost function J that accounts for the geography of representation uncertainty (Forget and Wunsch, 2007; Forget, 2010; Forget et al., 2015a). In principle, average cost function values near one are expected when the climatology estimate is an optimal fit to the data, indicating that it is neither an overfit (J<1) nor a suboptimal fit (J>1). Strict interpretation of absolute cost function values however assumes that uncertainty specifications are perfect (Forget and Wunsch, 2007; Forget, 2010; Forget et al., 2015a). In practice, optimality can only be achieved iteratively and approximately by reducing large-scale misfits to observations, e.g. via the adjoint method as done in ECCO (Forget, 2010; Forget et al., 2015a; Forget and Ponte, 2015; Forget et al., 2015b).

The agreement between OCCA2.2D and Argo (Fig. A8) is near $J = 1$ and stationary through time (red curves). It is also closer to Argo than OCCA1 (blue curves) and ECCO4 (not shown). Looking at $J(\text{OCCA1})$ through time, its increase is a measure of observed climate trends and variability over the Argo period (recalling that OCCA1 is a climatology for 2004-2006, Forget, 2010). In contrast, OCCA2 misfits are rather stationary, which reflects that these solutions largely reproduce observed climate fluctuations and trends in the ocean (Forget and Ponte, 2015). The reduction from $J(\text{OCCA2.2A})$ to $J(\text{OCCA2.2B})$ provides a measure of biases that had accumulated during the spin-up phase of OCCA2.2A. In turn, the reduction from $J(\text{OCCA2.2B})$ to $J(\text{OCCA2.2C})$ is from the time-mean adjustment based on Argo, which does not contribute to relative SOL-EI .

The fact that $J(\text{OCCA2.2C})$ and $J(\text{OCCA2.2D})$ are so close to each other across the Argo period confirms that OCCA2.2 largely captures observed changes even before the addition of $\delta\mathbb{T}^{inter}_{O2.2c\rightarrow O2.2}$ in Eq. A11, which is generally a small term (Figs. 1-2 , A6-A9).

Looking forward, we suggest that further reducing the magnitude of this non-conservative term would help further improve our understanding of SOL-EI . To this end, one could use the ECCO4 inverse estimation machinery e.g. by penalizing $\delta\mathbb{T}^{inter}_{O2.2c\rightarrow O2.2}$ in the cost function and re-optimizing model parameters (Forget et al., 2015a, b; Forget and Ponte, 2015). Appropriately setting up such an estimation experiment would require careful consideration of least-square weights for $\delta\mathbb{T}^{inter}_{O2.2c\rightarrow O2.2}$, and running it would induce significant computational cost. However, we hope that the present paper will provide a rationale and a useful jumping off point to motivate such research.

https://doi.org/10.5194/egusphere-2026-4643
Preprint. Discussion started: 6 August 2026

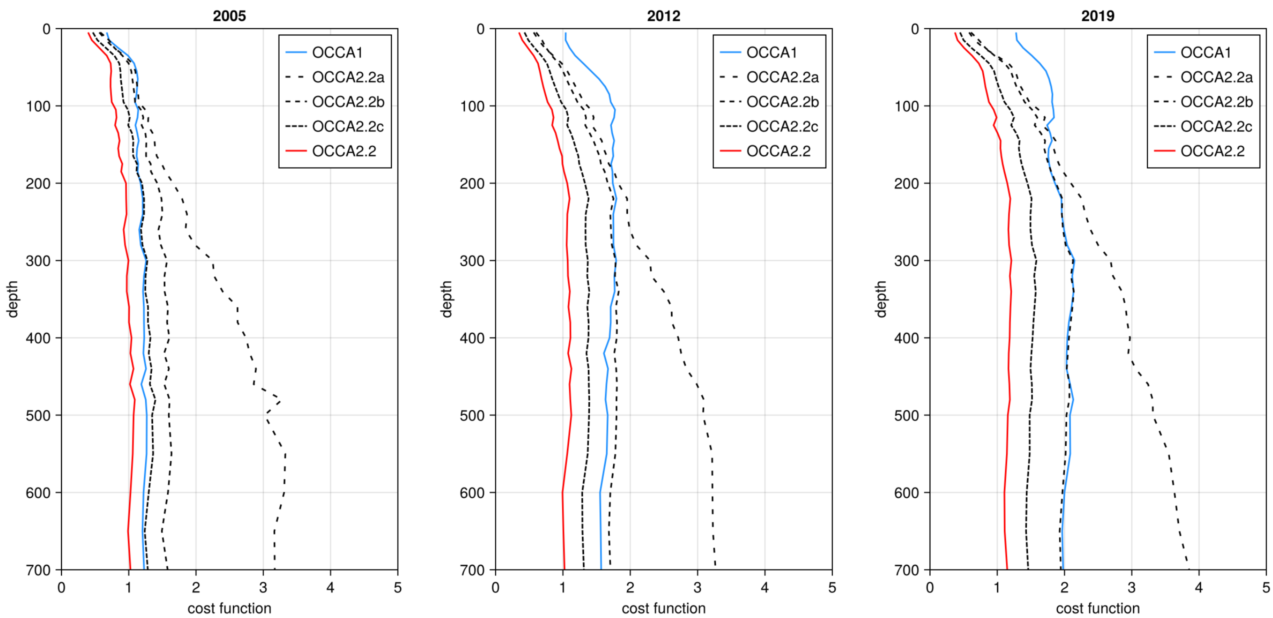

Figure A8. Mean cost functions that measure misfits to Argo for different ocean state estimates and different years. These sample mean cost function values were computed over all Argo profiles collected over the global ocean. In theory, they would be near 1 if a true optimum had been reached and error estimates were perfect (Forget and Wunsch, 2007). In practice, it is the comparison of cost function values across estimates that is of most interest (Forget, 2010; Forget et al., 2015a, b).

https://doi.org/10.5194/egusphere-2026-4643
Preprint. Discussion started: 6 August 2026

A9 Heat Budget Uncertainty Quantification

The trend in Argo-based adjustments – i.e., the difference between OCCA2.2D and OCCA2.2C – is a concrete measure of uncertainties that affect the closed heat budget estimate (Figs. A9). This is a relatively small term for both the SOL and in the layer below (200m-2000m), with minor effects on SOL-EI or its geography predicted by the closed heat budget estimate (OCCA2.2A or OCCA2.2B).

To assess OHC uncertainties beyond the Argo period, we can also compare OCCA2.2A to the IAPV4 temperature reanalysis (Cheng et al., 2024b) which uses other types of ocean temperature data. There is again a good agreement between the two estimates, OCCA2.2A and IAPV4, for global mean time series (Fig. 2) and spatio-temporal averages (Figs. A10). Hence we conclude that the closed heat budget estimate from OCCA2.2A provides a useful approximation and mechanistic interpretation for decadal trends in ocean heat content over the extended 1980-2022 period. While comparison with other IAPV4-like products for the SOL is left outside the scope of this paper, the reader is referred to recent intercomparison studies that have focused on EEI (Minière et al., 2023; Hakuba et al., 2024; Meyssignac et al., 2024).

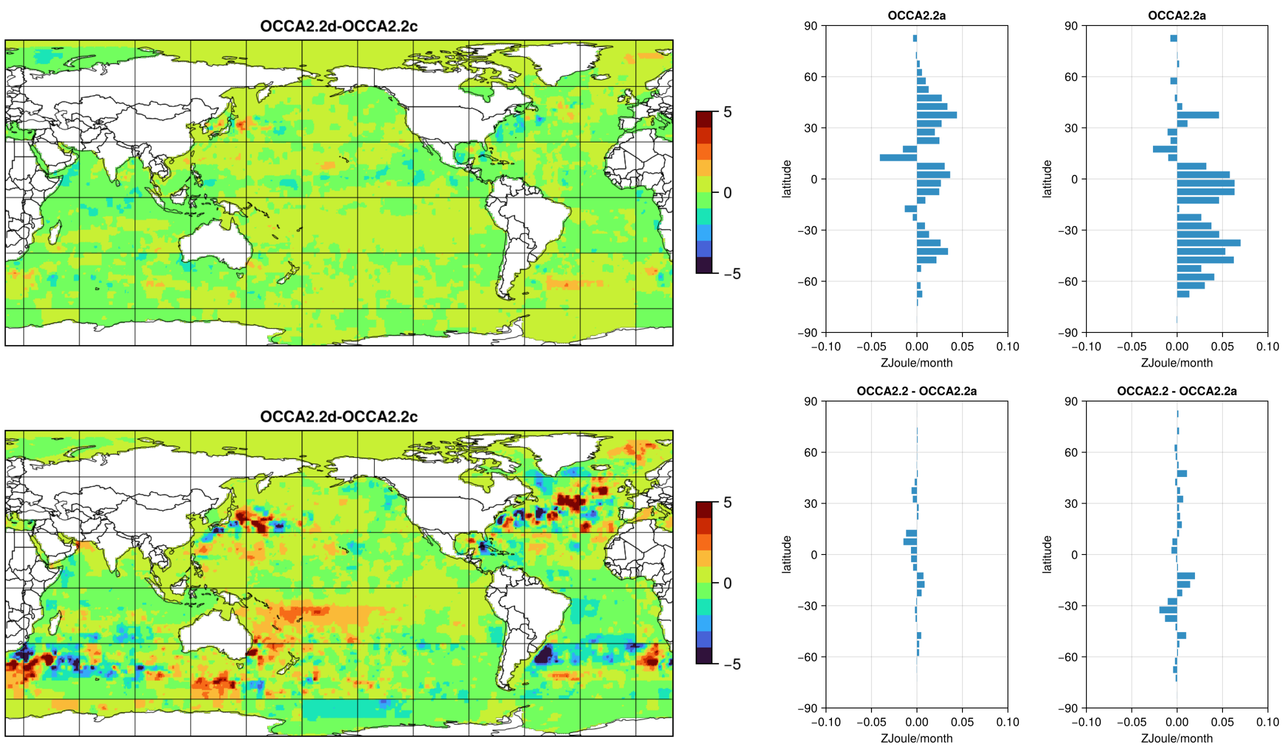

Figure A9. Heat content tendency anomaly for the SOL (top left) and for the 200-2000m depth range (bottom left), calculated over 2013:2022 from the difference between OCCA2.2D and OCCA2.2C, in W/m2. Right panels : integrated over 5 degree latitude bands, in ZJoule/Month.

https://doi.org/10.5194/egusphere-2026-4643
Preprint. Discussion started: 6 August 2026

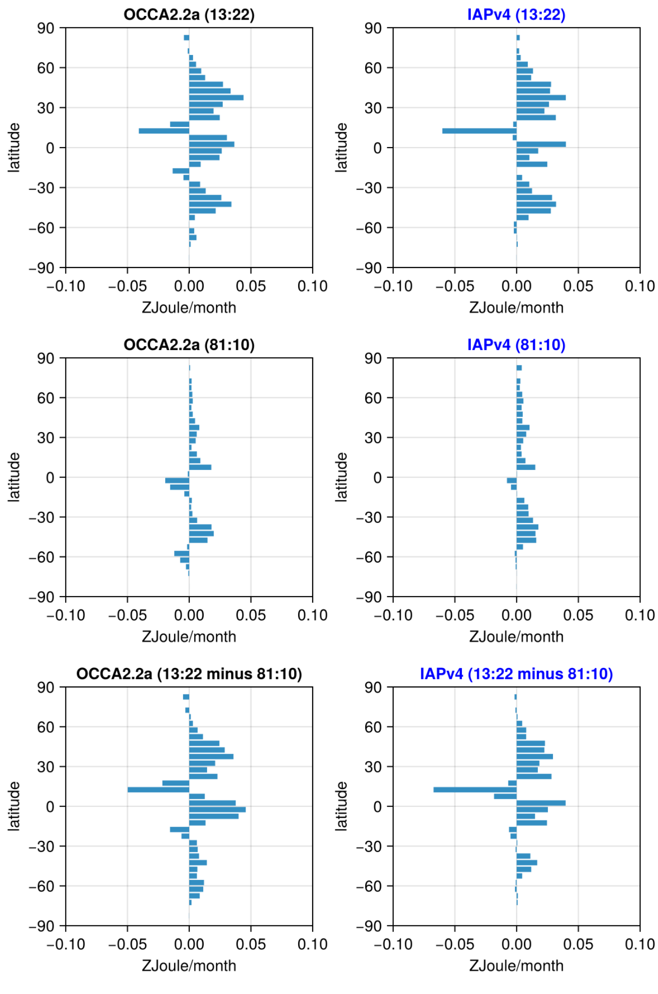

Figure A10. Mean SOL heat content trend estimates for 2013:2022 (top), 1981:2010 (middle), and the difference. Units : ZJoule/month.

https://doi.org/10.5194/egusphere-2026-4643
Preprint. Discussion started: 6 August 2026

A10 Downward Shortwave Profile

To delimit the SOL we choose 200m depth as a simple representation of the bottom of the euphotic layer, based upon the
520 exponential decay of available solar radiation with depth (Fig. A11). This choice could be worth revisiting in future study because the euphotic depth can vary depending on location, and uncertainty can arise due to discrepancies between various estimation methods (Wu et al., 2021). But until a consensus may emerge that there was a better and simple choice, we'd advocate for using a 200m depth limit to estimate SOL-HB and SOL-EI . This approach readily provides a needed framework for mechanistic interpretation and meaningful comparison with SST-based and Argo-based estimates. It also yields a convenient,
525 two-dimensional, view of the euphotic layer to quantify impacts of global warming on marine ecosystems.

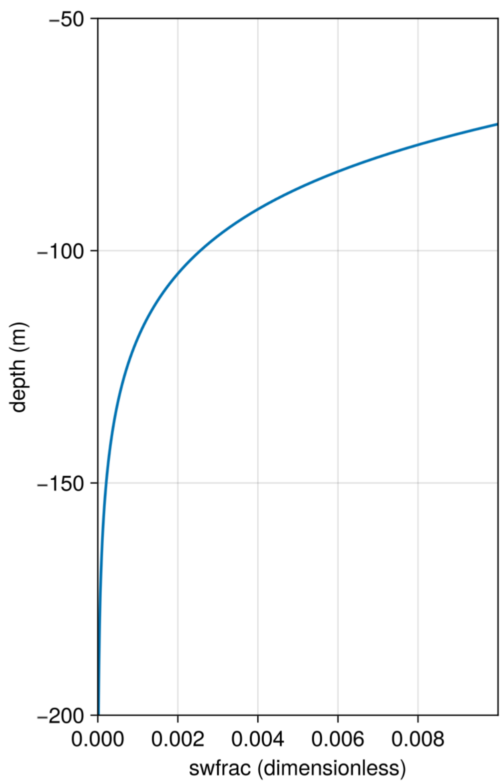

Figure A11. Fraction of downward shortwave radiation (swfrac) that reaches a certain depth, as approximated in the ECCO4 model.

https://doi.org/10.5194/egusphere-2026-4643
Preprint. Discussion started: 6 August 2026

Author contributions. GF designed the study and methods; carried out the simulations, computations, analyses; wrote the paper.

Acknowledgements. GF acknowledges support from NASA awards 80NSSC20K0796, 80NSSC23K0355, 80NSSC22K1697, 1676067, and 1686358. GF is also grateful to Jane Chapin for proof-reading this manuscript.

https://doi.org/10.5194/egusphere-2026-4643
Preprint. Discussion started: 6 August 2026

References

Anderson, S., Barton, A., Clayton, S., Dutkiewicz, S., and Rynearson, T.: Marine phytoplankton functional types exhibit diverse responses to thermal change, Nature communications, 12, 1–9, 2021.

Armour, K. C., Marshall, J., Scott, J. R., Donohoe, A., and Newsom, E. R.: Southern Ocean warming delayed by circumpolar upwelling and equatorward transport, Nature Geoscience, 9, 549–554, https://doi.org/10.1038/ngeo2731, 2016.

Asch, R. G., Stock, C. A., and Sarmiento, J. L.: Climate change impacts on mismatches between phytoplankton blooms and fish spawning phenology, Global Change Biology, 25, 2544–2559, https://doi.org/https://doi.org/10.1111/gcb.14650, 2019.

Bagnell, A. and DeVries, T.: 20th century cooling of the deep ocean contributed to delayed acceleration of Earth's energy imbalance, Nature Communications, 12, https://doi.org/10.1038/s41467-021-24472-3, 2021.

Capotondi, A., Rodrigues, R. R., Sen Gupta, A., Benthuysen, J. A., Deser, C., Frölicher, T. L., Lovenduski, N. S., Amaya, D. J., Le Grix, N., Xu, T., Hermes, J., Holbrook, N. J., Martinez-Villalobos, C., Masina, S., Roxy, M. K., Schaeffer, A., Schlegel, R. W., Smith, K. E., and Wang, C.: A global overview of marine heatwaves in a changing climate, Communications Earth and Environment, 5, 701, https://doi.org/10.1038/s43247-024-01806-9, 2024.

Cheng, L., Abraham, J., Trenberth, K. E., Boyer, T., Mann, M. E., Zhu, J., Wang, F., Yu, F., Locarnini, R., and Fasullo, J.: New Record Ocean Temperatures and Related Climate Indicators in 2023, Advances in Atmospheric Sciences, pp. 1–15, 2024a.

Cheng, L., Pan, Y., Tan, Z., Zheng, H., Zhu, Y., Wei, W., Du, J., Yuan, H., Li, G., Ye, H., Gouretski, V., Li, Y., Trenberth, K. E., Abraham, J., Jin, Y., Reseghetti, F., Lin, X., Zhang, B., Chen, G., Mann, M. E., and Zhu, J.: IAPv4 ocean temperature and ocean heat content gridded dataset, Earth System Science Data, 16, 3517–3546, https://doi.org/10.5194/essd-16-3517-2024, 2024b.

Church, J. A., White, N. J., and Arblaster, J. M.: Significant decadal-scale impact of volcanic eruptions on sea level and ocean heat content, Nature, 438, 74–77, https://doi.org/10.1038/nature04237, 2005.

Dogar, M. M., Sato, T., and Liu, F.: Ocean sensitivity to periodic and constant volcanism, Scientific Reports, 10, 293, 2020.

ECCO Consortium, Fukumori, I., Wang, O., Fenty, I., Forget, G., Heimbach, P., and Ponte, R. M.: Synopsis of the ECCO Central Production Global Ocean and Sea-Ice State Estimate, Version 4 Release 4, https://doi.org/10.5281/zenodo.4533349, 2021.

England, M. H., McGregor, S., Spence, P., Meehl, G. A., Timmermann, A., Cai, W., Gupta, A. S., McPhaden, M. J., Purich, A., and Santoso, A.: Recent intensification of wind-driven circulation in the Pacific and the ongoing warming hiatus, Nature Climate Change, 4, 222–227, https://doi.org/10.1038/nclimate2106, 2014.

Feng, J., Stige, L. C., Hessen, D. O., Zuo, Z., Zhu, L., and Stenseth, N. C.: A threshold sea-surface temperature at 14° C for phytoplankton nonlinear responses to ocean warming, Global Biogeochemical Cycles, 35, e2020GB006 808, 2021.

Forget, G.: Mapping ocean observations in a dynamical framework: A 2004-06 ocean atlas, Journal of Physical Oceanography, 40, https://doi.org/10.1175/2009JPO4043.1, 2010.

Forget, G. and Ferreira, D.: Global ocean heat transport dominated by heat export from the tropical Pacific, Nature Geoscience, https://doi.org/10.1038/s41561-019-0333-7, 2019.

Forget, G. and Ponte, R.: The partition of regional sea level variability, Progress in Oceanography, 137, https://doi.org/10.1016/j.pocean.2015.06.002, 2015.

Forget, G. and Wunsch, C.: Estimated global hydrographic variability, Journal of Physical Oceanography, 37, https://doi.org/10.1175/JPO3072.1, 2007.

https://doi.org/10.5194/egusphere-2026-4643
Preprint. Discussion started: 6 August 2026

Forget, G., Ferron, B., and Mercier, H.: Combining Argo profiles with a general circulation model in the North Atlantic. Part 1: Estimation of hydrographic and circulation anomalies from synthetic profiles, over a year, Ocean Modelling, 20, https://doi.org/10.1016/j.ocemod.2007.06.001, 2008a.

Forget, G., Mercier, H., and Ferron, B.: Combining Argo profiles with a general circulation model in the North Atlantic. Part 2: Realistic transports and improved hydrography, between spring 2002 and spring 2003, Ocean Modelling, 20, https://doi.org/10.1016/j.ocemod.2007.06.002, 2008b.

Forget, G., Campin, J.-M., Heimbach, P., Hill, C. N., Ponte, R. M., and Wunsch, C.: ECCO version 4: an integrated framework for non-linear inverse modeling and global ocean state estimation, Geoscientific Model Development, 8, 3071–3104, https://doi.org/10.5194/gmd-8-3071-2015, 2015a.

Forget, G., Ferreira, D., and Liang, X.: On the observability of turbulent transport rates by Argo: Supporting evidence from an inversion experiment, Ocean Science, 11, https://doi.org/10.5194/os-11-839-2015, 2015b.

Forget, G., Winkelbauer, S., Song, Y., Mayer, M., Bourdalle-Badie, R., and Yang, X.: Quantifying Uncertainties in ocean heat transports and budgets using an ensemble of observational state estimates, Journal of Climate, in prep.

Frankignoul, C. and Hasselmann, K.: Stochastic climate models, Part II Application to sea-surface temperature anomalies and thermocline variability, Tellus A: Dynamic Meteorology and Oceanography, 29, 289, https://doi.org/10.3402/tellusa.v29i4.11362, 1977.

Frölicher, T. L., Sarmiento, J. L., Paynter, D. J., Dunne, J. P., Krasting, J. P., and Winton, M.: Dominance of the Southern Ocean in Anthropogenic Carbon and Heat Uptake in CMIP5 Models, Journal of Climate, 28, 862 – 886, https://doi.org/10.1175/JCLI-D-14-00117.1, 2015.

Fyfe, J. C., Gillett, N. P., and Zwiers, F. W.: Overestimated global warming over the past 20 years, Nature Climate Change, 3, 767–769, 2013.

Gonzales, K. R., Swain, D. L., Nardi, K. M., Barnes, E. A., and Diffenbaugh, N. S.: Recent warming of landfalling atmospheric rivers along the west coast of the United States, Journal of Geophysical Research: Atmospheres, 124, 6810–6826, 2019.

Gu, D. and Philander, S. G. H.: Interdecadal Climate Fluctuations That Depend on Exchanges Between the Tropics and Extratropics, Science, 275, 805–807, https://doi.org/10.1126/science.275.5301.805, 1997.

Gu, P., Liu, Z., and Delworth, T. L.: Strong oceanic forcing on decadal surface temperature variability over global ocean, Geophysical Research Letters, 51, e2023GL107 401, 2024.

Hakuba, Fourest, Boyer, Meyssignac, Carton, Forget, Cheng, Giglio, Johnson, Kato, Killick, Kolodziejczyk, Kuusela, Landerer, Llovel, Locarnini, Loeb, Lyman, Mishonov, Pilewskie, Reagan, Storto, Sukianto, , and von Schuckmann: Trends and Variability in Earth's Energy Imbalance and Ocean Heat Uptake since 2005, Surveys in Geophysics, https://doi.org/10.1007/s10712-024-09849-5, 2024.

Hansen, J., Ruedy, R., Sato, M., and Lo, K.: Global surface temperature change, Reviews of Geophysics, 48, 2010.

Henley, B. J., Gergis, J., Karoly, D. J., Power, S., Kennedy, J., and Folland, C. K.: A Tripole Index for the Interdecadal Pacific Oscillation, Climate Dynamics, 45, 3077–3090, https://doi.org/10.1007/s00382-015-2525-1, 2015.

Hersbach, H., Bell, B., Berrisford, P., Hirahara, S., Horányi, A., Muñoz-Sabater, J., Nicolas, J., Peubey, C., Radu, R., and Schepers, D.: The ERA5 global reanalysis, Quarterly Journal of the Royal Meteorological Society, 146, 1999–2049, 2020.

Hersh, C., Wijffels, S., Gebbie, G., and Forget, G.: The Long Lives of Subducted Spice and Vorticity Anomalies in the Subtropical Oceans, Journal of Physical Oceanography, 55, 131 – 153, https://doi.org/10.1175/JPO-D-24-0081.1, 2025.

Holbrook, N. J., Scannell, H. A., Sen Gupta, A., Benthuysen, J. A., Feng, M., Oliver, E. C., Alexander, L. V., Burrows, M. T., Donat, M. G., and Hobday, A. J.: A global assessment of marine heatwaves and their drivers, Nature communications, 10, 2624, 2019.

Jiang, W., Forget, G., Song, Y., and Haine, T.: Coupled air-sea interaction drove and sustained the 2013–2016 North Pacific Marine Heatwave, Nature Communications, in press.

Knutson, T. R., Chung, M. V., Vecchi, G., Sun, J., Hsieh, T.-L., and Smith, A.: Climate change is probably increasing the intensity of tropical cyclones, in: Critical issues in climate change science, https://doi.org/https://doi.org/10.5281/zenodo.4570333, 2021.

Kosaka, Y. and Xie, S.-P.: Recent global-warming hiatus tied to equatorial Pacific surface cooling, Nature, 501, 403–407, https://doi.org/10.1038/nature12534, 2013.

Levitus, S., Antonov, J. I., Boyer, T. P., Baranova, O. K., Garcia, H. E., Locarnini, R. A., Mishonov, A. V., Reagan, J. R., Seidov, D., Yarosh, E. S., and Zweng, M. M.: World ocean heat content and thermosteric sea level change (0–2000 m), 1955–2010, Geophysical Research Letters, 39, https://doi.org/https://doi.org/10.1029/2012GL051106, 2012.

Li, G., Cheng, L., Zhu, J., Trenberth, K. E., Mann, M. E., and Abraham, J. P.: Increasing ocean stratification over the past half-century, Nature Climate Change, 10, 1116–1123, 2020.

Li, Z., England, M. H., and Groeskamp, S.: Recent acceleration in global ocean heat accumulation by mode and intermediate waters, Nature Communications, 14, 6888, https://doi.org/10.1038/s41467-023-42468-z, 2023a.

Li, Z., England, M. H., and Groeskamp, S.: Recent acceleration in global ocean heat accumulation by mode and intermediate waters, Nature Communications, 14, 6888, 2023b.

Liu, C., Allan, R. P., Mayer, M., Hyder, P., Desbruyères, D., Cheng, L., Xu, J., Xu, F., and Zhang, Y.: Variability in the global energy budget and transports 1985–2017, Climate Dynamics, 55, 3381–3396, https://doi.org/10.1007/s00382-020-05451-8, 2020.

Loeb, N. G., Johnson, G. C., Thorsen, T. J., Lyman, J. M., Rose, F. G., and Kato, S.: Satellite and Ocean Data Reveal Marked Increase in Earth's Heating Rate, Geophysical Research Letters, 48, https://doi.org/https://doi.org/10.1029/2021GL093047, 2021.

Long, Y., Guo, X., Holbrook, N. J., Yan, Y., Liu, Z., and Zhu, X.-H.: Importance of ocean dynamics in the onset and persistence of the 2013-15 and 2019-20 northeast Pacific marine heatwaves, Nature Communications, 16, https://doi.org/10.1038/s41467-025-64873-2, 2025.

Medhaug, I., Stolpe, M. B., Fischer, E. M., and Knutti, R.: Reconciling controversies about the 'global warming hiatus', Nature, 545, 41–47, https://doi.org/10.1038/nature22315, 2017.

Meyssignac, Fourest, Mayer, Johnson, Calafat, Ablain, Boyer, Cheng, Desbruyeres, Forget, Giglio, Kuusela, Locarnini, Lyman, Llovel, Mishonov, Reagan, Rousseau, and Benveniste: North Atlantic heat transport convergence derived from a regional energy budget using different ocean heat content estimates, Surveys in Geophysics, https://doi.org/10.1007/s10712-024-09865-5, 2024.

Meyssignac, B., Boyer, T., Zhao, Z., Hakuba, M. Z., Landerer, F. W., Stammer, D., Köhl, A., Kato, S., L'Ecuyer, T., Ablain, M., Abraham, J. P., Blazquez, A., Cazenave, A., Church, J. A., Cowley, R., Cheng, L., Domingues, C. M., Giglio, D., Gouretski, V., Ishii, M., Johnson, G. C., Killick, R. E., Legler, D., Llovel, W., Lyman, J., Palmer, M. D., Piotrowicz, S., Purkey, S. G., Roemmich, D., Roca, R., Savita, A., Schuckmann, K. v., Speich, S., Stephens, G., Wang, G., Wijffels, S. E., and Zilberman, N.: Measuring Global Ocean Heat Content to Estimate the Earth Energy Imbalance, Frontiers in Marine Science, 6, https://doi.org/10.3389/fmars.2019.00432, 2019.

Minière, A., von Schuckmann, K., Sallée, J.-B., and Vogt, L.: Robust acceleration of Earth system heating observed over the past six decades, Scientific Reports, 13, 22 975, 2023.

Oliver, E. C., Benthuysen, J. A., Darmaraki, S., Donat, M. G., Hobday, A. J., Holbrook, N. J., Schlegel, R. W., and Sen Gupta, A.: Marine Heatwaves, Annual Review of Marine Science, 13, 313–342, https://doi.org/10.1146/annurev-marine-032720-095144, 2021.

Piecuch, C. G., Heimbach, P., Ponte, R. M., and Forget, G.: Sensitivity of contemporary sea level trends in a global ocean state estimate to effects of geothermal fluxes, Ocean Modelling, 96, 214–220, https://doi.org/https://doi.org/10.1016/j.ocemod.2015.10.008, 2015.

Rahmstorf, S., Jendrkowiak, J., Gou, R., Cheng, L., Ruiz-Angulo, A., and Björnsson, H.: Multidecadal Atlantic "Warming Hole" Heat Content Variations Are Caused by Ocean Heat Transport, Not by Surface Fluxes, Geophysical Research Letters, 53, https://doi.org/10.1029/2025gl118383, 2026.

Reagan, J. R., Boyer, T. P., García, H. E., Locarnini, R. A., Baranova, O. K., Bouchard, C., Cross, S. L., Mishonov, A. V., Paver, C. R., and Seidov, D.: World ocean atlas 2023, NOAA National Centers for Environmental Information. Dataset: NCEI Accession, 270533, 2024.

Roemmich, D., Church, J., Gilson, J., Monselesan, D., Sutton, P., and Wijffels, S.: Unabated planetary warming and its ocean structure since 2006, Nature Climate Change, 5, 240–245, https://doi.org/10.1038/nclimate2513, 2015.

Roemmich, D., Alford, M. H., Claustre, H., Johnson, K., King, B., Moum, J., Oke, P., Owens, W. B., Pouliquen, S., Purkey, S., Scanderbeg, M., Suga, T., Wijffels, S., Zilberman, N., Bakker, D., Baringer, M., Belbeoch, M., Bittig, H. C., Boss, E., Calil, P., Carse, F., Carval, T., Chai, F., Conchubhair, D., d'Ortenzio, F., Dall'Olmo, G., Desbruyeres, D., Fennel, K., Fer, I., Ferrari, R., Forget, G., Freeland, H., Fujiki, T., Gehlen, M., Greenan, B., Hallberg, R., Hibiya, T., Hosoda, S., Jayne, S., Jochum, M., Johnson, G. C., Kang, K., Kolodziejczyk, N., Körtzinger, A., Traon, P.-Y. L., Lenn, Y.-D., Maze, G., Mork, K. A., Morris, T., Nagai, T., Nash, J., Garabato, A. N., Olsen, A., Pattabhi, R. R., Prakash, S., Riser, S., Schmechtig, C., Schmid, C., Shroyer, E., Sterl, A., Sutton, P., Talley, L., Tanhua, T., Thierry, V., Thomalla, S., Toole, J., Troisi, A., Trull, T. W., Turton, J., Velez-Belchi, P. J., Walczowski, W., Wang, H., Wanninkhof, R., Waterhouse, A. F., Waterman, S., Watson, A., Wilson, C., Wong, A. P. S., Xu, J., and Yasuda, I.: On the Future of Argo: A Global, Full-Depth, Multi-Disciplinary Array, Frontiers in Marine Science, 6, https://doi.org/10.3389/fmars.2019.00439, 2019.

Rousselet, L., Cessi, P., and Forget, G.: Coupling of the mid-depth and abyssal components of the global overturning circulation according to a state estimate, Science Advances, 7, eabf5478, https://doi.org/10.1126/sciadv.abf5478, 2021.

Salinger, M., Renwick, J., and Mullan, A.: Interdecadal Pacific Oscillation and South Pacific climate, International Journal of Climatology, 21, 1705–1721, https://doi.org/https://doi.org/10.1002/joc.691, 2001.

Sallée, J.-B., Pellichero, V., Akhoudas, C., Pauthenet, E., Vignes, L., Schmidtko, S., Garabato, A. N., Sutherland, P., and Kuusela, M.: Summertime increases in upper-ocean stratification and mixed-layer depth, Nature, 591, 592–598, 2021.

Scannell, H. A., Johnson, G. C., Thompson, L., Lyman, J. M., and Riser, S. C.: Subsurface Evolution and Persistence of Marine Heatwaves in the Northeast Pacific, Geophysical Research Letters, 47, e2020GL090 548, https://doi.org/https://doi.org/10.1029/2020GL090548, e2020GL090548 2020GL090548, 2020.

Sen Gupta, A., Thomsen, M., Benthuysen, J. A., Hobday, A. J., Oliver, E., Alexander, L. V., Burrows, M. T., Donat, M. G., Feng, M., Holbrook, N. J., Perkins-Kirkpatrick, S., Moore, P., Rodrigues, R., Scannell, H., Taschetto, A., Ummenhofer, C., Wernberg, T., and Smale, D.: Drivers and impacts of the most extreme marine heatwave events, Scientific reports, 10, 1–15, 2020.

Song, Y. and Forget, G.: Ocean heat pathways and transports associated with ENSO, Journal of Climate, in prep.

Song, Y. and Forget, G.: Temperature Change in Mode Water Source Regions, Journal of Climate, under review.

Song, Y., Li, Y., Forget, G., Hu, A., Li, Q., Shi, J.-R., Chen, X., Ge, K., and Wang, F.: Inter-basin contrast in the Southern Ocean warming, Nature Communications, 16, 9063, 2025.

Speer, K. and Forget, G.: Global distribution and formation of mode waters, vol. 103, https://doi.org/10.1016/B978-0-12-391851-2.00009-X, 2013.

Trenberth, K. E., Fasullo, J. T., and Kiehl, J.: Earth's global energy budget, Bulletin of the American Meteorological Society, 90, 311–324, 2009.

https://doi.org/10.5194/egusphere-2026-4643
Preprint. Discussion started: 6 August 2026

Vernier, J.-P., Thomason, L. W., Pommereau, J.-P., Bourassa, A., Pelon, J., Garnier, A., Hauchecorne, A., Blanot, L., Trepte, C., Degenstein, D., and Vargas, F.: Major influence of tropical volcanic eruptions on the stratospheric aerosol layer during the last decade, Geophysical Research Letters, 38, https://doi.org/https://doi.org/10.1029/2011GL047563, 2011.

von Schuckmann, K., Minière, A., Gues, F., Cuesta-Valero, F. J., Kirchengast, G., Adusumilli, S., Straneo, F., Ablain, M., Allan, R. P., Barker, P. M., Beltrami, H., Blazquez, A., Boyer, T., Cheng, L., Church, J., Desbruyeres, D., Dolman, H., Domingues, C. M., García-García, A., Giglio, D., Gilson, J. E., Gorfer, M., Haimberger, L., Hakuba, M. Z., Hendricks, S., Hosoda, S., Johnson, G. C., Killick, R., King, B., Kolodziejczyk, N., Korosov, A., Krinner, G., Kuusela, M., Landerer, F. W., Langer, M., Lavergne, T., Lawrence, I., Li, Y., Lyman, J., Marti, F., Marzeion, B., Mayer, M., MacDougall, A. H., McDougall, T., Monselesan, D. P., Nitzbon, J., Otosaka, I., Peng, J., Purkey, S., Roemmich, D., Sato, K., Sato, K., Savita, A., Schweiger, A., Shepherd, A., Seneviratne, S. I., Simons, L., Slater, D. A., Slater, T., Steiner, A. K., Suga, T., Szekely, T., Thiery, W., Timmermans, M.-L., Vanderkelen, I., Wjiffels, S. E., Wu, T., and Zemp, M.: Heat stored in the Earth system 1960–2020: where does the energy go?, Earth System Science Data, 15, 1675–1709, https://doi.org/10.5194/essd-15-1675-2023, 2023.

Watanabe, M., Kang, S. M., Collins, M., Hwang, Y.-T., McGregor, S., and Stuecker, M. F.: Possible shift in controls of the tropical Pacific surface warming pattern, Nature, 630, 315–324, https://doi.org/10.1038/s41586-024-07452-7, 2024.

Wu, J., Lee, Z., Xie, Y., Goes, J., Shang, S., Marra, J. F., Lin, G., Yang, L., and Huang, B.: Reconciling between optical and Biological determinants of the euphotic zone depth, Journal of Geophysical Research: Oceans, 126, e2020JC016 874, 2021.

Wu, Q. and Gregory, J. M.: Estimating Ocean Heat Uptake Using Boundary Green's Functions: A Perfect-Model Test of the Method, Journal of Advances in Modeling Earth Systems, 14, e2022MS002 999, https://doi.org/https://doi.org/10.1029/2022MS002999, e2022MS002999 2022MS002999, 2022.

Wu, Q., Zhang, X., Church, J. A., and Hu, J.: ENSO-Related Global Ocean Heat Content Variations, Journal of Climate, 32, 45 – 68, https://doi.org/10.1175/JCLI-D-17-0861.1, 2019.

Wu, Q., Gregory, J. M., Zanna, L., and Khatiwala, S.: Time-varying global energy budget since 1880 from a reconstruction of ocean warming, Proceedings of the National Academy of Sciences, 122, https://doi.org/10.1073/pnas.2408839122, 2025.

Yang, C., Bourdallé-Badie, R., Drevillon, M., Amaya, D., Aouf, L., Aydogdu, A., Barton, B., Bell, M., Boyer, T., Blauw, A., Carton, J., Candela, T., Cossarini, G., Dabrowski, T., de Boisseson, E., de Mora, L., Fablet, R., Forget, G., Fujii, Y., Garric, G., Giunta, V., Salamon, P., Hersbach, H., Juza, M., Sommer, J. L., Martin, M., McAdam, R., Garcia, M. M., Morim, J., Nicolì, D., Reppucci, A., Samuelsen, A., Sauzède, R., Slivinski, L., Specq, D., Storto, A., Tuomi, L., Vandenbulcke, L., Aznar, R., Beuvier, J., Cipollone, A., Clementi, E., Biagio, V. D., Escudier, R., Giesen, R., Greiner, E., Guihou, K., Korabel, V., Lamouroux, J., Chune, S. L., Lellouche, J.-M., Levier, B., Lima, L., Mangin, A., Mayer, M., Melet, A., Miraglio, P., Oikonomou, C., Pfeffer, J., Renshaw, R., Ringgaard, I., Thual, S., Titaud, O., Tonani, M., van Gennip, S., von Schuckmann, K., Drillet, Y., and Traon, P.-Y. L.: Gathering users and developers to shape together the next-generation ocean reanalyses: Ocean reanalyses workshop of the European Copernicus Marine Service, Bulletin of the American Meteorological Society, https://doi.org/10.1175/BAMS-D-24-0034.1, 2024.

Zanna, L., Khatiwala, S., Gregory, J. M., Ison, J., and Heimbach, P.: Global reconstruction of historical ocean heat storage and transport, Proceedings of the National Academy of Sciences, 116, 1126–1131, https://doi.org/10.1073/pnas.1808838115, 2019.